“DYNAMIC ANALYSIS OFELECTROSTATICALLY EXITED MICRO CANTILEVER BEAM”

A Thesis Submitted in partial fulfillment
of the requirements for the award of

Master of Technology

In

Machine Design and Analysis

By

J S N B Vamsee Gowtham A

Roll No: 209ME1179

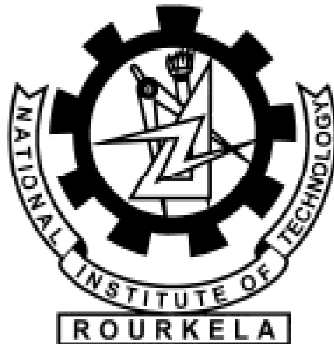

Department of Mechanical Engineering
National Institute of Technology-Rourkela
Rourkela -769008
2011

“DYNAMIC ANALYSIS OFELECTROSTATICALLY EXITED MICRO CANTILEVER BEAM”

A Thesis Submitted in partial fulfillment
of the requirements for the award of

Master of Technology

In

Machine Design and Analysis

By

J S N B Vamsee Gowtham A

Roll No: 209ME1179

Under the Guidance of

Dr. J.Srinivas

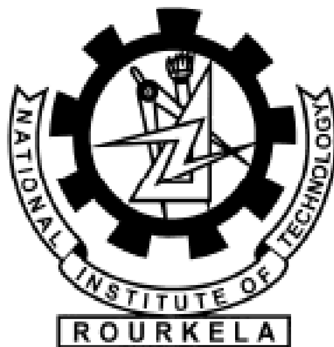

Department of Mechanical Engineering
National Institute of Technology
Rourkela

2011

NATIONAL INSTITUTE OF TECHNOLOGY
ROURKELA

CERTIFICATE

This is to certify that the thesis entitled, **"DYNAMICANALYSIS OFELECTROSTATICALLY EXITED MICRO CANTILEVER BEAM"** by **Mr. J S N B Vamsee Gowtham A** in partial fulfillment of the requirements for the award of **Master of Technology** Degree in ***Mechanical Engineering*** with specialization in "**Machine Design & Analysis**" at the National Institute of Technology, Rourkela is an authentic work carried out by him under my supervision and guidance.

To the best of my knowledge the matter embodied in the thesis has not been submitted to any other University/ Institute for the award of any Degree or Diploma.

Date:

Dr. J. Srinivas
Dept. of Mechanical Engineering
National Institute of Technology
Rourkela-769008

ACKNOWLEDGEMENT

Successful completion of this work will never be one man’s task. It requires hard work in right direction. There are many who have helped to make my experience as a student a rewarding one.

In particular, I express my gratitude and deep regards to my thesis guide **Prof. J. Srinivas,** first for his valuable guidance, constant encouragement and kind co-operation throughout period of work which has been instrumental in the success of thesis.

I also express my sincere gratitude to **Prof. R. K. Sahoo**, Head of the Department, Mechanical Engineering, for providing valuable departmental facilities.

Finally, I would like to thank my fellow post-graduate students.

J S N B Vamsee Gowtham A

Roll No. 209ME1179

Department of Mechanical Engineering

National Institute of Technology

Rourkela

CONTENTS

Abstract i

Nomenclature

Chapter 1 -Introduction

1.1 Overview of MEMS 1

1.2 Applications of microbeam Resonators 2

1.3 Types of actuation systems 3

1.3.1 Electrostatic actuation 4

1.3.2 Piezoelectric actuation 5

1.3.3 Magnetic actuation 5

1.4 Scope of the present work 6

Chapter 2 -Literature Review

2.1 Pull-in instability analysis 8

2.2 Transient chaotic dynamics 10

2.3 Pull-in and chaos control 13

Chapter 3 Single degree of freedom model

3.1 Mathematical formulation of equation of motion 18

3.2 Expression for squeeze-film damping 19

3.3 Electrostatic excitation 21

3.4 Non-dimensonalization 22

3.5 Stability analysis 24

3.6 Results and discussions 25

3.6.1 Dynamic pull-in curves 26

3.6.2 Frequency responses with pressure variation 31

3.6.3 Frequency responses with ac voltage variation 33

Chapter 4 Distributed parameter modelling

4.1 Mathematical formulation of equation of motion 36

4.2 Normalization procedure 38
4.3 Reduced order model 40
4.4 Results and discussions 42
4.5 Control of chaotic dynamics 49
Chapter 5 Conclusions
5.1 Summary 50
5.2 Future scope 50
References 52
Appendix 55

ABSTRACT

Microcantilever beams find applications in modern micro and nano devices, such as, microswitches, microvalves and atomic force microscopes (AFM). These are generally fabricated from single crystal silicon. Dynamics and pull-in analysis of these cantilever resonators (Beams) is of vital importance before their fabrication. Microbeams are often actuated by several actuation techniques such as piezoelectric, electromagnetic, thermal and electrostatic excitations. In electrostatic actuation a controlled dc voltage is applied together with a harmonic or suddenly applied ac component. The electrostatic force is in fact a non-linear function of displacement of the beam. In such beams when electrostatic force exceeds the elastic restoring force in the beam contact between the beam and supporting substrate occurs. This situation is referred to as pull-in instability which defines the life of a resonator. The study of pull-in is very important to design process of microsystems, such as, microgyroscopes to analyze the frequency response, the dynamic range and sensitivity.

In this line, present work attempts to predict the static and dynamic characteristics of a cantilever microbeam resonator. A single-DOF model incorporating squeeze-film damping forces is first considered. Dynamic pull-in voltages are obtained from time-domain analysis and phase trajectories, for values of ac voltage amplitudes. Parametric studies are carried-out to find the effect of ac voltage amplitudes and air film pressure on the intermediate stability of system. For this bifurcation analysis and Poincare maps are employed. The harmonic voltage frequency effects are also illustrated in the form of frequency-response curves. As stiffness of test structure reduces due to applied voltage, the spring –softening behavior is observed in frequency-response curves. Two benchmark cantilever beam geometries available in literature are considered to illustrate the approach.

For validation of lumped-parameter SDOF model, an approximate solution for the continuous beam system used in Galerkin's method is adopted. One mode approximation upto fifth order terms is formulated to arrive the dynamic pull-in curves and frequency response diagrams. Results are compared for the two test cases.

Finally the sliding mode-control approach is implemented to convert chaotic motion of resonator to a desired periodic motion. The non-linear dynamic equations are solved using

Runge-Kutta fourth order time-integration explicit scheme. The integral of cantilever mode shape functions, phase trajectories and Poincare maps obtained with MATLAB programs. The organization of thesis is as follows: Chapter-1 presents overall introduction to microresonators highlighting their importance in various devices. Chapter-2 gives brief description of literature available in this field. Chapter-3 presents mathematical model and corresponding results with respect to Single-DOF oscillator model. Chapter-4 deals with Galerkin’s approach and its output results. Chapter-5 gives overall conclusions of the work.

Nomenclature

L	Length of microbeam (μm)
b	Width of the microbeam (μm)
d, g	Initial gap (μm)
m	Mass of the microbeam (kg)
ρ	Density of microbeam (kg/m^3)
y,w	Deflection of microbeam (μm)
E	Young's modulus (GPa)
υ	Poisson's ratio
A	Base area of electrode $(\mu m)^2$
A_1	Cross-sectionl areaof micrbeam$(\mu m)^2$
c_v	Viscous damping coefficient (N-s/m)
c(y)	Squeeze film damping coefficient (N-s/m)
k	Structural stiffness of microbeam (N/m)
ε_0	Permittivity in free space (F/m)
ε_r	Relative permittvity of air
V_{dc}, V_p	dc voltage
V_{Ac}, V_0	ac voltage
F_e	Electrostatic force developed per unit length
ω_1	First natural frequency (rad/s)
ω	Frequency of ac signal (rad/s)
K_n	Knudsen number
$\sigma(y)$	Squeeze-film number
μ_{eff}	Effective dynamic viscosity (Pa-s)
p_0	Working pressure (Pa)
p_a	Ambient pressure (Pa)
λ	Mean free path of gas molecule (μm)
C	Capacitance for the microbeam
r	Frequency ratio
ϕ	Mode shape function

CHAPTER-1

1. INTRODUCTION

This chapter presents a brief introduction to microelectromechanical systems, microresonators and various types of materials, actuation schemes and objectives of the present work.

1.1 Overview of MEMS

Microelectromechanical System (MEMS) is a new research frontier due to its multiple physical fields properties. Micro-Electro-Mechanical Systems (MEMS) is the integration of mechanical elements, sensors, actuators, and electronics on a common silicon substrate through the utilization of microfabrication technology. While the electronics are fabricated using integrated circuit (IC) process sequences, the micromechanical components are fabricated using compatible “micromachining” processes that selectively etch away the parts of the silicon wafer or add new structural layers to form the mechanical and electromechanical devices. Micro switches and resonators are simple Micro-Electro-Mechanical System elements, used in several sensors and actuators. Technology of Micro-Electro-Mechanical systems (MEMS) has experienced a lot of progress recently. Their light weight, low cost, small dimensions, low-energy consumption and durability attracted them widely. Compared to the traditional mechanical systems, the MEMS devices are usually small and their largest size will not exceed 1 cm, sometimes only in micron order. Studying the design parameters of Micro-Electro-Mechanical by scientific techniques is of great importance; therefore simulation tools are being improved.

Micromachining can be done for materials such as silicon, glass, ceramics, polymers, and compound semiconductors made of group III and V elements and a variety of metals including titanium and tungsten. Silicon, however, remains the material of choice for microelectromechanical systems.

Among the various materials available silicon can be economically manufactured in single crystal substrates. This crystalline nature provides many significant electrical and mechanical advantages. Electrical conductivity of the silicon makes use of impurity doping which is a very core operation of electronic semiconductor devices. Mechanically, silicon is an elastic and robust material. Over the last few decades the tremendous wealth of information

accumulated on silicon and its compounds has made it possible to innovate and explore new areas of application extending beyond the manufacturing of electronic integrated circuits.

It becomes evident that silicon is a best suitable base material on which electronic, mechanical, thermal, optical, and even fluid-flow functions can be integrated. Ultrapure, electronic-grade silicon wafers available for the integrated circuit industry are most common in the MEMS technology. The relatively low cost of these substrates makes them very attractive for the fabrication of micromechanical components and systems.

Silicon is a very good thermal conductor with a thermal conductivity greater than that of many metals available. Its conductivity is approximately 100 times larger than that of glass. In most of the complex integrated systems, the silicon substrate can be used as an efficient heat sink. Due to these wide advantages mono crystalline silicon is used as material in MEMS fabrication both as a substrate and as a structural material for MEMS devices. The elastic behaviour of silicon depends on the orientation of structure. The possible values of Young's modulus ranges from 130 to 188 GPa and those for Poisson ratio range from 0.048 to 0.4.

The three major operations involved in MEMS are:

1) Sensing: It is an important operation that is used to measure the mechanical input by converting it to an electrical signal e.g a MEMS accelerometer or a pressure sensor. (could also measure electrical signals as in the case of Current Sensors)
2) Actuation: Using an electrical input signal to cause the displacement (or rotation) of a mechanical structure e.g A synthetic Jet Actuator.
3) Power Generation: Generates power from a available mechanical input e.g MEMS Energy Harvesters.

These three operations require some form of transduction schemes such as piezoelectric, electrostatic, piezoresistive, electrodynamic, Magnetic and Magnetostrictive.

1.2 Applications of Microbeam Resonators

Microbeam resonators find wide applications in the field of medicine, automobiles, printing. Resonators are the MEMS device components which are well known for their

parametric excitation during the application of electrostatic forces. A resonator is a mechanical structure designed to vibrate at a particular resonant frequency. Resonators can be fabricated from a range of single crystal materials with micron-sized dimensions using various micromachining processes such as surface and bulk-micromachining. The resonant frequencies of such microresonators are extremely stable, enabling them to be used as a time base (the quartz tuning fork in watches, for example) or as the sensing element of a resonant sensor. Resonant microbeams (resonators) have been widely used as transducers in mechanical microsensors since the mid-1980s. As interest grew dramatically in MEMS devices for wireless communications applications and the demand for high-frequency and quality factor resonators increased rapidly, MEMS resonators were proposed in the mid-1990s as a feasible alternative to conventional large-size resonators. Microresonators find wide application in micro switches, amplifiers, sensors and accelerometers. Capacitive accelerometers are utilized in automobiles for safety purpose in seat belts. Fig.1.1 shows one such a vibrating resonator accelerometer.

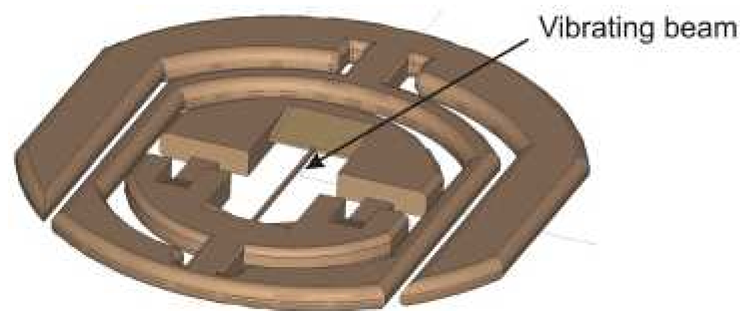

Fig.1.1 Vibrating inertial accelerometer transducer

Accelerometer sensor MMA means Micro Machined Accelerometer. Micro Machined technologies have capabilities of sensing the rate of change of velocity or acceleration. In cars, accelerometer sensor continuously monitors the rate of change of acceleration and accordingly it gives input to microcontroller where microcontroller scans this value with programmed values. If acceleration is more than the programmed value it triggers the actuator. MMA1260 senses the acceleration in only one direction i.e. in Z direction whereas MMA7260 senses the acceleration in three direction i.e. in X, Y and Z directions. The microcantilevers also find application in Atomic Force Microscope (AFM). The microcantilever used in AFM plays an important role for the high resolution scanning enabling the resolution on the order of a nanometer. i.e. more than 1000 times better than optical diffraction limit. Comb drives which consists of series of

microbeams can also be used for the actuation purpose in the MEMS devices. Comb-drives are linear motors that utilise electrostatic forces acting between two metal combs. While comb drives built at normal human scales (size) are extremely inefficient there is the potential to minimize them to microscopic or nanoscale devices where more common designs will not function. Almost all comb-drives are built on the micro or nano scale and are typically manufactured using silicon. Thus, micro-resonators are an integral part of many MEMS devices (RF filters, mass sensors and AFM). Electrostatic actuation with a dc voltage superimposed to an ac harmonic voltage is common way to actuate these resonators.

1.3 Types of actuation systems

MEMS often involve movable parts, requiring some microactuators. These microactuation requires mechanical energy so as to obtain a vibrating or translating or rotating motion based on the requirement for our MEMS device. The various types of actuation techniques that are used in are electrostatic, magnetic, piezoelectric etc. In-spite of all the available actuation techniques we prefer electrostatic actuation because of its ease in the control and high current density. The advantages of electrostatic actuation include relatively large displacement, ease of fabrication and controllable linearity of actuation. The voltage that which we maintain is the control parameter for the forces developed in the actuation.

1.3.1 Electrostatic actuation

An electric charge is created around the electric field due to potential difference between two conductors. This electric field applies a force between them. This principle, widely known since Maxwell's era, has not been so much used during the past decades, but MEMS have a high interest in using electrostatic actuators. The force is computed by differentiating with respect to gap g, the energy per unit length stored in the capacitor. That is

$$F_e = -\frac{1}{2}V^2\frac{\partial C_g}{\partial g} = \frac{\varepsilon_0\varepsilon_r}{2}\frac{bV^2}{(g_0 - w)^2} \tag{1.1}$$

Here C_g is capacitive per unit length, V is voltage difference between 2 bodies. C_g comprises of parallel-plate capacitance and fringing field capacitance.

The main problem of electrostatic effect is that it decreases with the square of the distance between the two charged bodies. In microscopic scale, this is a huge advantage, because most of the structures have a very low aspect ratio (i.e. width and length are large before thickness and gap in z direction), so the distance between bodies is really very small. Electrostatics is the most widely used force in the design of MEMS. In industry, it is used in microresonators, switches, micromirrors, accelerometers, etc. Almost every kind of microactuator has one or more electrostatic actuation based version. Electrostatic actuation introduces nonlinear behavior such as hysteresis, jump and dynamic instabilities. This nonlinear behaviour is used in many devices suchas ultrasensitive mass-sensors, switches with low actuation voltage etc.

1.3.2 Piezoelectric actuation

Piezoelectric materials, called familiarly piezo, are materials that show a small strain when they're placed under an electric field. This small strain is not so useful at macroscale, but at a micro scale, this becomes very interesting source.

The piezoelectric effect is realized as the linear electromechanical interaction between the mechanical and the electrical state in crystalline materials with no inversion symmetry. The piezoelectric effect is a reversible process in that materials exhibiting the direct piezoelectric effect (the internal generation of electrical charge resulting from an applied mechanical force) also exhibit the reverse piezoelectric effect (the internal generation of a mechanical force resulting from an applied electrical field). Actuators based on piezoelectric ceramic material prime movers (or piezo-actuators) are finding broad acceptance in applications where precision motion and/or high frequency operation is required. Piezoactuators can produce smooth continuous motion with resolution levels at the nanometer and subnanometer level. This property makes them useful in precision positioning and scanning systems. Piezoelectricity is found in useful applications such as the production and detection of sound, generation of high voltages, electronic frequency generation, microbalances, and ultrafine focusing of optical assemblies. It is also the basis of a number of scientific instrumental techniques with atomic resolution, the scanning probe microscopes. Atomic force microscope is one among those.

1.3.3 Magnetic actuation

A plate is supported by torsional hinge structure of embedded conducting wires, constituting multi windings positioned at different locations. The conducting wires of these windings are therefore of different lengths. Two permanent magnets are placed on the side of the plate, such that the magnetic field lines are parallel to the plane and orthogonal to the torsional hinges. When current passes through the coils, Lorentz forces will develop and cause rotational torque on the plate. The direction of the torque depends on the direction of input currents. A MEMS magnetic Actuator is a device that uses the MEMS process technology to convert an electrical signal (current) into a mechanical output (displacement) by employing the well known Lorentz Force Equation or the theory of Magnetism. When a current-carrying Conductor is placed in a static magnetic field, the field produced around the conductor interacts with the static field to produce a force. This Force can be used to cause the displacement of a mechanical structure.

1.4 Scope of the present work

Based on available techniques, in the present work, an electrostatically excited resonator is selected for analysis. Here as dc voltage steadily increased the amplitudes of oscillation of elastic structure increases up to certain critical value. When the applied voltage increases beyond a critical value, called pull-in voltage, the elastic force can no longer resist the electrostatic force, leading thereby to collapse of the structure. That is structure falls on to the substrate. The MEMS structures are liable to this instability known as the pull-in instability. A key issue in the design of such a device is to tune the electric load away from the pull-in instability which leads to collapse of the microbeam and hence the failure of the device. In the present work, initially the pull-in voltages are predicted for microcantilever resonator subjected to both dc polarization voltage and harmonic ac voltage. By calculating the pull-in values for a particular system considered, the operating region of microcantilever beam resonator is predicted. After predicting pull-in voltage it is necessary to know the periodic and non periodic operating regions of resonator under various operating variables. Time domain and phase plane diagrams are used to determine the region where the system can be operated safely without any instability.

Single DOF and one-mode-continuous system approximations are employed to know the dynamic response and stability regions of electrostatically actuated micro cantilever beam

resonator. Squeeze-film damping forces of air between substrate and beam are considered with two dimensional Reynold's equation. An expression for damping coefficient is adopted in terms of squeeze number, absolute viscosity, air pressure and Knudsen number. The entire work is classified into three broad headings:

i. Prediction of dynamic pull-in voltages from time-domain responses, study the variation of natural frequency with applied voltages.
ii. Analyze the stability of resonator as a function of ac harmonic voltage and air pressure in the gap.
iii. Analyze the sliding-mode control strategy is convert any aperiodic states into desired periodic output. Fig.1.2 shows the block diagram of the proposed scheme.

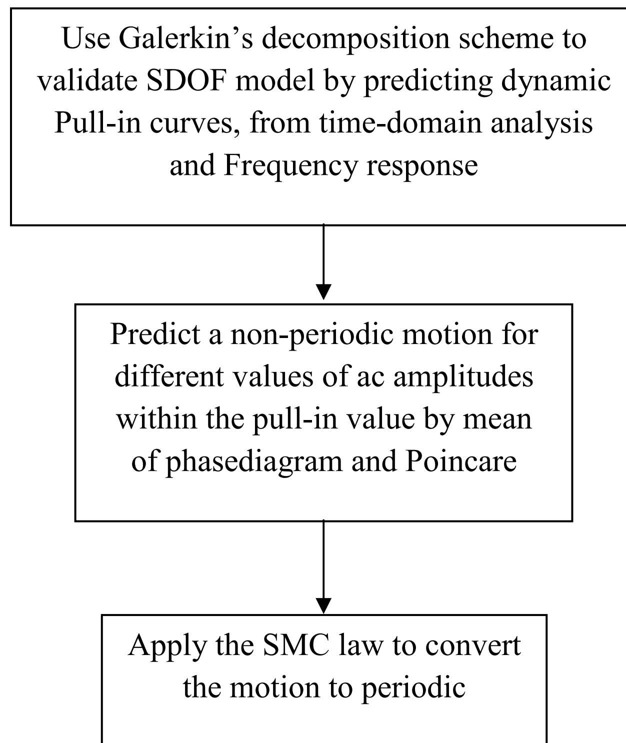

Fig.1.2 Block diagram of the various stages

Computer programs are implemented for each task in MATLAB environment. Results are validated with two benchmark examples from literature.

CHAPTER-2

2. LITERATURE REVIEW

This chapter is intended for reporting list of several available works on microbeam resonator studies, starting from pull-in analysis to chaotic motion control. Many researchers have investigated the nonlinear dynamical behaviors of micro-cantilever based instrument in MEMS under various loading conditions. Recent works highlighted the importance of resonator beam dynamics. All these works are classified into three broad headings:

i. Pull-in analysis
ii. Transient analysis
iii. Control of resonators

2.1 Pull-in Instability studies.

This section classifies the work under pull-in instability analysis, squeeze-film damping models and reduced-order modeling approaches.

Ouakad and Younis [1] presented an investigation of the nonlinear dynamics of carbon nanotubes when actuated by both ac and dc load. Dynamic analysis is conducted to explore the nonlinear oscillation of carbon nanotube near its fundamental natural frequency. The carbon nanotube is described by an Euler–Bernoulli beam model that accounts for the geometric nonlinearity and the nonlinear electrostatic force. A reduced-order model based on the Galerkin method is developed and utilized to simulate the static and dynamic responses of the carbon nanotube. The nonlinear analysis is carried out using a shooting technique to capture periodic orbits combined with the Floquet theory to analyze their stability. Subharmonic-resonances are found to be activated over a wide range of frequencies, which is a unique property of CNTs. The complex nonlinear dynamics phenomena, such as hysteresis, dynamic pull-in, hardening and softening behaviors and frequency bands with an inevitable escape from a potential well are presented.

Lee *et al*. [2] proposed an improved theoretical approach to predict the dynamic behavior of long, slender and flexible microcantilevers affected by squeeze-film damping at low ambient pressures. Theoretical frequency response functions are derived for a flexible microcantilever beam excited both inertially and via external forcing. They investigated the relative importance of theoretical assumptions made in the Reynolds-equation-based approach for flexible

microelectromechanical systems. The uncertainties in damping ratio prediction introduced due to assumptions on the gas rarefaction effect, gap height and pressure boundary conditions are studied. They attempted to calculate squeeze-film damping ratios of higher order bending modes of flexible microcantilevers in high Knudsen number regimes by theoretical method.

Nayfeh and Younis [3] studied the pull-in instability in microelectromechanical(MEMS) resonators and found that the characteristics of the pull-in phenomenon in the presence of AC loads differ from those under purely DC loads. They analyzed this phenomenon, dubbed dynamic pull-in, and formulated safety criteria for the design of MEMS resonant sensors and filters excited near one of their natural frequencies. This phenomenon is utilized to design a low-voltage MEMS RF switch actuated with a combined DC and AC loading. The frequency or the amplitude of the AC loading can be adjusted to reduce the driving voltage and switching time. The new actuation method has the potential of solving the problem of high driving voltages of RF MEMS switches. The reduced-order model with minimum of three modes are employed used to predict the transient and steady-state responses.

Yagubizade *et al*. [4] presented the squeeze-film damping effects on the dynamic response of electrostatically-actuated clamped-clamped microbeams. They utilized the coupled nonlinear Euler-Bernoulli beam equation (1D) and the nonlinear Reynolds equation (2D). A Galerkin-based reduced-order model and finite difference method have been used for beam and Reynolds equations respectively. They also considered the nonlinearity effect of squeeze-fluid near the pull-in voltage. So, from the nonlinearity behavior in large deflection, single equivalent value consideration for damping ratio or quality factor is incorrect and cannot predict its behavior exactly and so it must be solved the beam or plate equation coupled with Reynolds equation. In their study made theoretically calculated pull-in voltages and pull-in times are in good agreement with available experimental data.

Huang *et al*. [5] investigated theoretically the squeeze-film damping and undergoing normal vibrations. Their model attempts to isolate viscous damping clearly from squeeze-film damping.

Bicak and Rao [6] presented an analytical method for the solution of squeeze film damping based on Green's function to the nonlinear Reynold's equation as a forcing term.

Approximate mode shapes of the rectangular plate are used to calculate the frequency shift and damping ratio.

Pasquale and Soma [7] studied the effects of electro-mechanical coupling on dynamic characterization of MEMS experimentally and analytically. The common experimental problems relating to dynamic characterization of electrostatically actuated Microsystems are described.

Alsaleem *et al*. [8] presented experimental and theoretical investigations of dynamic pull-in of an electrostatically actuated resonators. The regimes of ac forcing amplitude versus ac frequency are predicted where a resonator is forced to pull-in if operated within these regimes. Effects of initial conditions, ac excitation amplitude, ac frequency, excitation type and sweeping type are investigated.

Krylov [9] investigated the dynamic pull-in instability of double clamped microscale beams actuated by a suddenly applied distributed electrostatic force and subjected to nonlinear squeeze-film damping. Galerkin's decomposition model with undamped linear modes as base functions was adopted. Largest Lyapunov exponent used to evaluate the stability.

Gutschmidt [10] employed a nonlinear continuum model to describe a doubly clamped microbeam subjected to two cases of electromechanical actuation. He illustrated difference between various reduced-order models.

2.2 Transient Chaotic dynamics

Chaos is a state of system instability in which there is a strong attractor and system rarely returns to original state. In micro resonators, the beam undergoes sometimes chaotic motion during different conditions of ac voltage and gap pressures. This section presents related works available in literature.

Younis and Nayfeh [11] studied the nonlinear dynamic response of a microbeam that is actuated by a general electric load subject to an applied axial load, accounting for mid-plane stretching. Various vibration tools like perturbation method, the method of multiple scales, is used to obtain two first order nonlinear ordinary-differential equations that describe the modulation of the amplitude and phase of the response and its stability. The dc electrostatic load is found to affect the qualitative and quantitative nature of the frequency response curves,

resulting in either a softening or a hardening behavior. The results obtained show that an inaccurate representation of the system nonlinearities may lead to an erroneous prediction of the frequency response. Also this work presents that the non linear model is capable of simulating the mechanical behavior of microbeams for general operating conditions and for a wider range of applied electric loads.

Chaterjee and Pohit [12] formulated a comprehensive model of an electrostatically actuated microcantilever with larger gap between the electrodes. The model accounts the nonlinearities of the system arising out of electric forces, geometry of the deflected beam and the inertial terms. Static analysis is carried out to know the deflections and dynamic analysis with five modes is carried out to known frequencies. They have observed that the reduced order model exhibits good convergence when five or more number of modes is considered for the analysis.

Younis and Nayfeh [13] presented a method for simulating squeeze-film damping of microplates actuated by large electrostatic loads. The method uses nonlinear Euler's beam equation, Von-Karmann's plate equation and compressible Reynold's equation. Effect of pressure and electrostatic force on mode shapes, natural frequencies and quality factor were shown.

Zhang and Meng [14] presented the nonlinear responses and dynamics of the electrostatically actuated MEMS resonant sensors under two-frequency parametric and external excitations. For the combination resonance, response and dynamics of MEMS resonator are studied. The responses of the system at steady-state conditions and their stability are predicted using the method of multiple scales. The effect of varying the dc bias, the squeeze-film damping, cubic stiffness and ac excitation amplitude on the frequency response curves, resonant frequencies and nonlinear dynamic characteristics are examined. Nonlinear dynamic characteristics of microbeam based resonant sensors in MEMS are investigated.

Towfighian *et al*. [15] presented the closed –loop dynamics of a chaotic electrostatic microbeam actuator. Bifurcation diagrams are derived by sweeping ac voltage amplitudes and frequencies. Period doubling, one well and two well chaos, super harmonic resonances and on-off chaotic oscillations were found in frequency sweep.

Zhang and Meng [16] presented a simplified model for the purpose of studying the resonant responses nonlinear dynamics of idealized electrostatically actuated micro-cantilever based devices in micro-electro-mechanical systems (MEMS). The underlying linearized dynamics of a periodic or quasi-periodic system described by a modified nonlinear Mathieu equation. The harmonic balance method is applied to simulate the resonant amplitude frequency responses of the system under the combined parametric and forcing excitations. The resonance responses and nonlinearities of the system are studied under different parametric resonant conditions, applied voltages and various gaps between the capacitor plates. The possible effects of cubic nonlinear spring stiffness and nonlinear response resulting from the gas squeeze film damping on the system can be ignored are discussed in detail. The nonlinear dynamical behaviors are characterized using phase portrait. The investigation provided the nonlinear and chaotic characteristics of micro-cantilever based device in MEMS.

Ostaseviciusa *et al*. [17] reported the results of numerical analysis of squeeze-film damping effects on the vibrations of cantilever microstructure effects under free and forced vibrations. The operation of microelectromechanical systems (MEMS) with movable parts is strongly affected by a fluid–structure interaction. Microelectromechanical devices often operate in ambient pressure, therefore air functions as an important working fluid. The influence of air in MEMS devices manifests as viscous air damping, which can be divided into two categories: slide-film damping and squeeze-film damping. The usage of particular form of Reynolds equation for modelling air-damping effects in case of developed electrostatic microswitch is suggested.

Zhang and Zhao [18] presented the one-mode analysis method on the pull-in instability of micro-structure under electrostatic loading. The one-mode analysis is the combination of Galerkin method and Cardan solution of cubic equation. This one-mode analysis offers a direct computation method on the pull-in voltage and displacement. Multi-mode analysis on predicting the pull-in voltages for three different structures (cantilever, clamped–clamped beams and the plate with four edges simply-supported) studied here. For numerical multi-mode analysis, they have shown that, using the structural symmetry to select the symmetric mode can greatly reduce both the computation effort and the numerical fluctuation.

Younis *et al*. [19] proposed a novel approach to generate reduced order models (macromodels) for electrically actuated microbeam based MEMS and used them to study the static and dynamic behavior of these devices. Linear and nonlinear elastic restoring forces and the nonlinear electric forces generated by the capacitors are accounted. Here the macromodel uses few linear-undamped mode shapes of a straight microbeam as basis functions in a Galerkin procedure which is obtained by discretizing the distributed parameter system in order to reduce the complexity of the simulation and reduces significantly the computational time.

Chaterjee and Pohit [20] developed a semi analytical model of an electrostatic actuated microcantilever beam taking into account the dependency of the effective viscosity on variable gap spacing through changing Knudsen number. Quality factors of the system are obtained numerically by coupled-field FE analysis.

Batra *et al*. [21] analyzed the vibrations of a fixed-fixed narrow microbeam excited by electrostatic force. Electrostatic fringe-field and residual stress effects were considered. The results of approximate one degree-of-freedom model loaded with distributed force were compared with those of three-dimensional FE simulations.

Zamanian and Khadem [22] studied the stability of a microbeam under an electric actuation. The stability of microresonator is studied using phase-plane diagram and Poincare mapping. The prediction of possible chaotic behavior is studied using Melnikov theorem. It was observerd that the pull-in instability occurs before going into the chaotic behavior for their dimensions. That is the system does not realize any chaotic behavior.

Ibrahim *et al*.[23] presented the effects of common MEMS nonlinearities on their shock response-spectrum. A case study of capacitive accelerometer is selected to show theoretically and experimentally the effects of nonlinearities due to squeeze-film damping and electrostatic actuation.

2.3 Pull-in and Chaos control

Pull-in avoidance by varying ac voltages as well as conversion of dangerous unstable non-periodic states of resonator to periodic motion has been illustrated in several papers. This deals with this classification.

Haghighi and Markazi [24] investigated the chaotic dynamics of micro mechanical resonator with electrostatic forces on both sides. They obtained Phase diagram, Poincare map and bifurcation diagram from numerical analysis which are necessary to predict chaos. Bifurcation adopted in this study corresponds to a transient chaotic behavior of the system and with some further increasing of the AC voltage amplitude can lead to the persistent chaotic motion. Suppression of pull-in instability in MEMS using a high frequency actuation is presented. They have Utilized the Melnikov function, an analytical criterion for homoclinic chaos in the form of an inequality is written in terms of the system parameters. A robust adaptive fuzzy control algorithm for controlling the chaotic motion is applied to eliminate chaotic motion.

Lakrad and Belhaq [25] studied the effect of a high-frequency ac tension on the pull-in instability induced by a dc tension in a microelectromechanical system. Analysis of steady states of slow dynamic enables us to depict the effect of the ac voltage on the pull-in. They have shown that when the microstructure is in the pull-in instability situation, adding a high-frequency ac actuation can create a new attracting solution which can avoid the failure of the device. This result indicates that by implementing a HFV, pull-in instability can be prevented in capacitive MEMS operating in regimes with relatively large amplitude. Taking advantage of the results obtained, current efforts are directed analytically and numerically to control and suppress undesirable nonlinear characteristics in MEMS as dynamic pull-in and hysteresis.

Yau *et al*. [26] analyzed the chaotic behavior of a micromechanical resonator with electrostatic forces on both sides and investigated the control of chaos. Phase diagram and maxmum Lyapunov exponent are used to identify chaotic motion. Byusing Fuzzy-sliding mode control methods the chaotic motion was turned to periodic.

Alsaleem and Younis [27] investigated the stability and integrity of parallel-plate microelectromechanical systems resonators using a delayed feedback controller. Two case studies are investigated: a capacitive sensor made of cantilever beams with a proof mass at their tip and a clamped-clamped microbeam. Dover-cliff integrity curves and basin-of-attraction analysis are used for the stability assessment of the frequency response of the resonators for several scenarios of positive and negative gain in the controller. It is found that in the case of a positive gain, a velocity or a displacement feedback controller can be used to effectively enhance the stability of the resonators.

CHAPTER-3

3. SINGLE DEGREE OF FREEDOM MODEL

Electrostatic devices have received wide popularity in MEMS field because of the fact that they can be operated at high frequency, they give high energy density and almost infinite life. Cantilever beam (Fig.3.1) as movable electrode is the most common example. The Microcantilever beam that we consider is studied with two kinds mathematical models. First is the single degree-of-freedom spring-mass model with consideration of squeeze-film damping and electrostatic nonlinearity terms.

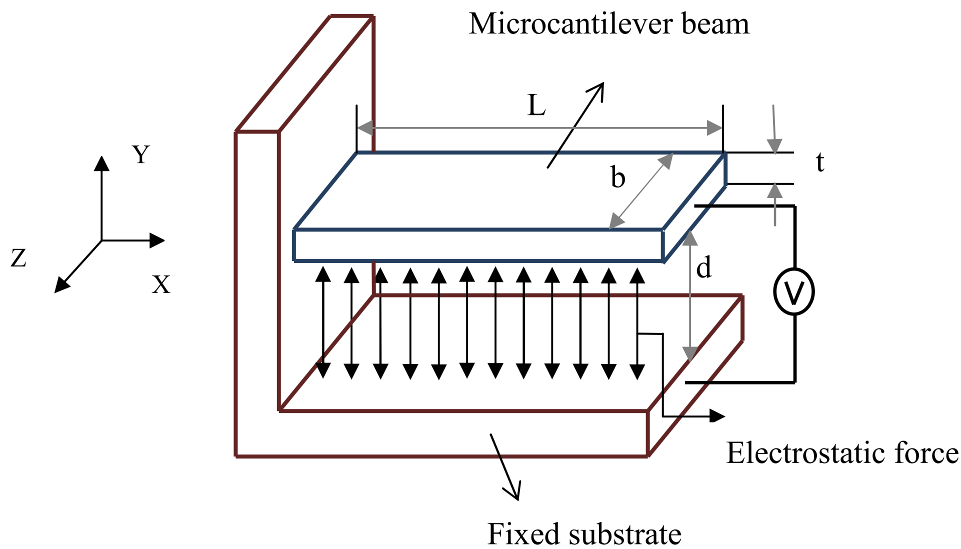

Fig.3.1 Physical setup of cantilever beam

The system comprises of two components. One is fixed and other movable. The fixed component is known as substrate. The substrate is the fixed supporting structure for the microbeam. Both movable microbeam and fixed substrate, both have electrodes. The movable component we considered here is of cantilever type which is made of silicon. A dc voltage (V_p) superimposed by harmonic ac voltage ($V_0 \cos\omega t$) is applied between the movable microbeam and the supporting substrate. Then the electrostatic force is produced between them make the microcantilever beam to oscillate with a particular amplitude relative to the applied voltage. Here $V= V_p+ V_0 \cos\omega t$. Microcantilever beam that we considered is modeled as a spring-mass system as shown in Fig.3.2 by considering damping into account.

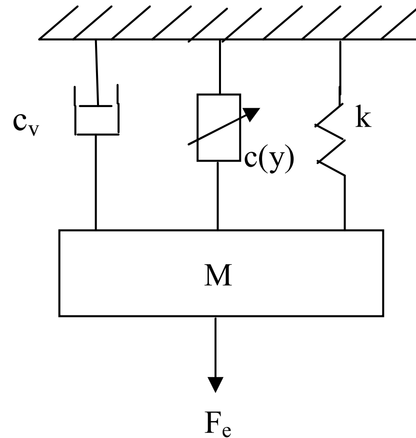

Fig.3.2 Pictorial representation of spring-mass model (m=ρAL, k=ω_1m)

Electrostatic actuation is provided for the spring-mass system and so the developed electrostatic force 'F_e' is responsible for the mass to come into motion. The spring-mass model internally has the structural resistance which acts in the direction opposite to the motion of the mass. Not only the structural resistance i.e. stiffness of the microbeam, but also the damping [c(y)+c_v] that opposes the motion of the mass. Damping in microstructures is also of special interest in the dynamic analysis of microbeams. The system which we consider posses both squeeze-film c(y) as well as viscous damping (c_v). Squeeze film damping is an important source of extrinsic damping. One of the important issues in MEMS modeling is simulation and characterization of the interaction between the vibrational structure with squeezed fluid between the structure and the substrate. When the system is undergoing the vibration, squeeze film damping starts acting. It occurs due to resistance of the viscous fluid present in between the beam and substrate. Squeeze film damping is dependent on the air-pressure (p_0) between substrate and beam surface. Corresponding to the particular pressure in the system the beam amplitude and behavior of system as well varies. This interaction of Squeeze-Film damping in microstructures strongly affects their characteristics especially their dynamic behavior. Thus, the system under study possesses these damping forces apart from the non-linear electrostatic force. Following section deals with the mathematical equations of motion and their dimensionless form.

The microcantilever beam that we considered is modeled as a spring-mass system as shown in Fig.3.2 by considering damping into account. Electrostatic actuation is provided for the

spring-mass system and so the developed electrostatic force 'F_e' is responsible for the mass to come into motion. The spring-mass model internally has the structural resistance which acts in the direction opposite to the motion of the mass. Not only the structural resistance i.e. stiffness of the microbeam, but also the damping [$c(y)+c_v$] that opposes the motion of the mass. Damping in microstructures is also of special interest in the dynamic analysis of microbeams. The system which we consider posses both squeeze-film $c(y)$ as well as viscous damping (c_v). Squeeze film damping is an important source of extrinsic damping. One of the important issues in MEMS modeling is simulation and characterization of the interaction between the vibrational structure with squeezed fluid between the structure and the substrate. When the system is undergoing the vibration, squeeze film damping starts acting. It occurs due to resistance of the viscous fluid present in between the beam and substrate. Squeeze film damping is dependent on the air-pressure between substrate and beam surface. Corresponding to the particular pressure in the system the beam amplitude and behavior of system as well varies. This interaction of Squeeze-Film damping in microstructures strongly affects their characteristics especially their dynamic behavior. Thus the system under study posses these damping forces apart from the non-linear electrostatic force.

3.1 Mathematical formulation of Equation of motion

The governing equation for a microcantilever beam resonator system subjected to electrostatic force under viscous damping is given by:

$$m\ddot{y} + c_v\dot{y} + ky = \frac{\varepsilon_o \varepsilon_r A(V_P + V_o cos\omega t)^2}{2(d-y)^2} \quad (3.1)$$

If the squeeze-film damping affect is also considered then the above equation of motion is modified as follows:

$$m\ddot{y} + [c(y) + c_v]\dot{y} + ky = \frac{\varepsilon_o \varepsilon_r A(V_P + V_o cos\omega t)^2}{2(d-y)^2} \quad (3.2)$$

The right hand term in the eqn.2.2 represents the electrostatic force required for the actuation. This electrostatic force is denoted by 'F_E'. Here ε_0 is permittivity of free space=8.8541878× 10^{-12}F/m, ε_r is relative permittivity=1 for air, A=b×L is cross section, d is initial gap.

$$F_E = \frac{\varepsilon_o \varepsilon_r A\left(V_P{}^2 + V_o{}^2 cos^2\omega t + 2V_P V_o cos\omega t\right)^2}{2(d-y)^2}$$

$$= \frac{\varepsilon_o \varepsilon_r A\left[\left(V_P{}^2 + \frac{V_o{}^2}{2}\right) + 2V_P V_o cos\omega t + \frac{V_o{}^2}{2} cos2\omega t\right]^2}{2(d-y)^2} \quad (3.3)$$

3.2 Expression for squeeze-film damping

Damping in the system is of important concern and its effect is studied for designing a system. Gas damping is the source of most MEMS and it is a strong function of viscosity. The absolute viscosity 'μ' is the ratio of the shear stress 'τ_0' between flow layers to the velocity gradient, through the fluid channel. The nature of viscosity of a liquid and the gas are different. Viscosity in liquid results from cohesion between adjacent molecules, but viscosity in a gas results from intermolecular collisions within the gas. As the molecular collisions rate depends on temperature in a gas, viscosity increases with temperature. In most of the macroscale engineering problems viscosity is unaffected by the pressure variations. However, when the distance between the micro beam and fixed substrate become comparable to the mean path ($d \approx \lambda$), the viscosity becomes sensitive to pressure variation. In this situation, molecular collisions rarely occur within the gas layer and the momentum is directly transferred between the gas molecules and MEMS surface, yielding a pressure-dependent viscosity.

Consider nonlinear Reynolds eq.

$$\nabla.\left(\frac{\rho d^3}{12\mu}\nabla p\right) = \frac{\partial}{\partial t}(\rho d) \quad (3.4)$$

where ∇p is pressure gradient, d is film thickness, μ is absolute viscosity, ρ is gas density.

At low ambient pressure or in very thin films, molecular interactions with surfaces need to be taken into account. The theory of rarefied gas flow developed by Knudsen (early 1900) is applied here. Veijola has given a function that approximates the pressure and film width dependency of viscosity in narrow gap. Based on different derivation considerations, one can get a different viscosity definition. The raynolds equation is applicable only in the continuum flow regime; the relationship between K_n and flow regimes is shown in Table 3.1

Table 3.1 Knudsen number and corresponding flow regimes

K_n	Flow regime	μ_{eff}/μ
< 0.01	Continuum	$0.956 < \mu_{eff}/\mu < 1$
$0.01<K_n<0.1$	Slip	$0.6 < \mu_{eff}/\mu < 0.956$
$0.1<K_n<10$	Transitional	$0.007 < \mu_{eff}/\mu < 0.6$
$K_n>10$	Molecular	$0 < \mu_{eff}/\mu < 0.007$

There are many types of damping which influence the dynamic properties of the system. Viscous damping, squeeze-film damping and slide-film damping are the few well known types of damping. By considering the viscous damping and squeeze-film damping for our system under consideration, the dynamic properties are analyzed. In order to increase the efficiency of actuation and improve the sensitivity of detection, the distance between the capacitor beams is minimized and the area of the electrode is maximized. Under such conditions, the so-called squeeze-film damping is pronounced. This phenomenon occurs as a result of the massive movement of the fluid underneath the beam, which is resisted by the viscosity of the fluid. This type of damping occurs frequently in MEMS devices. Blench model analytically solves the linearized Reynold's equation with trivial boundary condition. It is the squeeze-film damping coefficient is expressed by considering the first term in Blench series as follows:

$$c(y) = \frac{64\sigma p_a A}{\pi^6 w(d-y)}\left(\frac{2}{4+\frac{\sigma^2}{\pi^4}}\right)$$

$$= \frac{768\ \mu_{eff} A^2}{\pi^6 (d-y)^3} \frac{2}{\left\{4 + \left(\frac{\sigma(y)}{\pi^2}\right)^2\right\}} \tag{3.5}$$

where,

$$\sigma(y) = \frac{12 A \omega \mu_{eff}}{p_a (d-y)^2} \tag{3.6}$$

$$\mu_{eff} = \frac{\mu}{1 + 9.638 {K_n}^{1.159}} \tag{3.7}$$

$$K_n = \frac{\lambda}{d} = \frac{\lambda_0 p_a}{p_0 d} \tag{3.8}$$

y is vertical deflection of resonating beam having effective mass m, A is area of electrode, A_1 is the crosssection area of the microbeam, d is initial gap width, c(y) is squeeze film damping, b is viscous damping coefficient, k is effective linear mechanical stiffness of the system, K_n is knudsen number, λ is mean free path of gas molecule, p_0 is working pressure, p_a is ambient pressure (1.013bar), σ(y) is squeeze number, μ is nominal dynamic viscosity of air, μ_{eff} is the effective dynamic viscosity, ε_o is permittivity in free space, V_p is dc voltage, V_0 is ac voltage, ω is the frequency of ac signal, $\lambda_0 = 65nm$.

3.3 Principle of Electrostatic actuation

Various physical properties of different materials and their interactions are used to achieve the desired sensing and actuation in the Micro domain. For example, different actuation methods include thermo-actuation, use of shape memory alloy, piezo actuation, magnetostatic actuation and electrostatic actuation.

Among the different actuation principles, the electrostatic actuation is predominantly employed because of short response time, high energy densities, low power consumption and being compatible with integrated circuit processes. So, many microelectromechanical systems make use of electrostatic forces to actuate their micro-devices such as microcantilever beam.

The electrostatic force is obtained by applying dc polarization voltage superimposed by harmonic or sudden ac voltage between the microcantilever beam and the fixed substrate. In microswitch system dc polarization voltage causes beam to deflect whereas the both dc polarization voltage and harmonic ac voltage are considered. In a microresonator system in

which dc part is used to apply a constant deflection to microbeam and ac part is used to excite harmonic modes of microbeam about the constant position.

Due to the nonlinear nature of electrostatic forces, the electromechanical response of microcantilever beam considered is often nonlinear. This nonlinearity may cause loss of stability in the electromechanical response and may limit the range of stable states. These operating states are to be predicted inorder to operate the MEMS device which makes use of microcantilver beam resonator.

Because of the application of voltage between the movable microcantilever beam and the fixed substrate electric field in induced which is a cause for the electrostatic actuation. The microcantilever beam tends to move back and forth from the fixed substrate.

As in the case of parallel plate capacitor the capacitance for the movable cantilever microbeam is given by 'C'.

$$C = \frac{\varepsilon_0 A}{(d - y)} \tag{3.9}$$

The energy 'E' of a capacitor with a voltage 'V' across the movable microcantilver beam and fixed substrate is given by

$$E = \frac{1}{2}\frac{\varepsilon_0 A}{(d - y)}V^2 \tag{3.10}$$

The electrostatic force between the microcantilever beam electrode and substrate can be determined by differentiating the energy function, E with respect to the coordinate in the direction of the force. In essence, this is the potential energy term of Lagrange's equation.

$$\frac{\partial E}{\partial y} = F_E = -\frac{1}{2}\frac{\varepsilon_0 A}{(d - y)^2}V^2 \tag{3.11}$$

3.4 Non-dimensionalization of equation of motion

As it is more convenient to use non-dimensional form of eq. of motion, we introduce:

Let

$$1)\varepsilon_0\varepsilon_r = c_o, \tag{3.12}$$

$$2)\ \frac{768\ \mu_{eff} p_a A^2}{\pi^6} = c_1, \tag{3.13}$$

$$3)\ \left(\frac{12A\omega\mu_{eff}}{p_a \pi^2}\right)^2 = c_2. \tag{3.14}$$

Considering the following dimensionless variables:

$$\tau = \omega_o t, r = \frac{\omega}{\omega_o}, x = \frac{y}{d} \tag{3.15}$$

$$\alpha = \frac{c_o\left(V_p^2 + \frac{V_o^2}{2}\right)}{2md^3{\omega_o}^2}, \beta = \frac{2V_p V_o \alpha}{\left(V_p^2 + \frac{V_o^2}{2}\right)}, \gamma = \frac{\alpha V_o^2}{2\left(V_p^2 + \frac{V_o^2}{2}\right)} \tag{3.16}$$

$$\zeta = \frac{b}{2m\omega_o} \quad , \omega_o = 3.5156\sqrt{\frac{EI}{\rho A L^4}} \tag{3.17}$$

The governing equation 3.2 with respect to non-dimensional variable τ reduces to the following form:

$$x'' + \frac{1}{m\omega_o}\left[\frac{2c_1 d(1-x)}{4d^4(1-x)^4 + c_2}\right]x' - 2\zeta x' + x = \frac{\alpha}{(1-x)^2} + \frac{\beta}{(1-x)^2} cosr\tau + \frac{\gamma}{(1-x)^2} cos2r\tau \tag{3.18}$$

Rewriting the dynamic system of equations in state-space form using

$$x_1 = x, \qquad x_2 = x' \text{and } x_3 = r\tau \tag{3.19}$$

We get

$$x_1' = x_2 \tag{3.20}$$

$$x_2' = -x_1 - \frac{1}{m\omega_o}\left[\frac{2c_1 d(1-x_1)}{4d^4(1-x_1)^4 + c_2}\right]x_2 - 2\zeta x_2 + \frac{\alpha}{(1-x_1)^2} + \frac{\beta}{(1-x_1)^2} cosx_3 + \frac{\gamma}{(1-x_1)^2} cos2x_3 \tag{3.21}$$

$$x_3' = r \tag{3.22}$$

The a non-dimensional differential equations of motion in state space (3.20-3.22) are solved using the Runge-Kutta fourth order numerical technique with non-dimensional time ranging from 0 to 1000 in substeps of approximately 0.01. An interactive computer program is implemented in MATLAB so as to obtain the time histories and phase plane diagram corresponding to the input voltages.

3.5 Stability analysis

The purpose of the stability analysis is to check whether the movable electrode will remain within the stable equilibrium range or not corresponding to the voltages applied. If the net force approaches an unstable point, the electrodes would have the possibility to hit the fixed structures and/or brake away. The voltage at that point is known as pull-in voltage.

Interaction of electrostatic force with linear elastic force results in a phenomenon called pull-in instability, which limits the functionality. Initially pull-in voltages are to be predicted to find the operating zones for the MEMS cantilever beam resonator. In dynamic stability analysis, it is always ensured that the resonator maintains periodic motion. In order to know the periodicity status, one often ascertained with time-histories, phase trajectories (diagrams) and frequency response curves. Graphs that plot one state variable against another during a dynamic event, with time as a parameter, are very useful. They are called phase-plane plots and are routinely used to capture the behavior of systems with several state variables.

There is a class of nonlinear systems that have an even more complex behavior, called chaotic behavior. A characteristic of chaotic behavior is that the state of a system after an interval of time is highly sensitive to the exact initial state. That is, a chaotic system, if started from two initial states very close to each other, after time can be in states that are arbitrarily far away in the accessible phase space of the system. Chaotic systems can also undergo complex jumps between regions of phase space. So the intermediate choatic and quasi-perodic states are analyzed for different values of ac harmonic amplitudes and frequencies as well as squeeze-film pressure between the beam and substrate surfaces. In addition to the pull-in analysis, the vibration tools such as Poincare maps and bifurcation diagrams are helpful to distinguish between periodic and non-periodic motion, between different kinds of periodic motion and

between chaotic and truly random motion. Poincare maps are plotted in order to distinguish the periodic and non-periodic states easily when the beam is under motion.

Poincare map is a dotted phase diagram in which each dot represents the state of system at the end of one period. These dots or points may either be finite or forming a curve or irregularly spread-over the diagram. Poincare map with finite number of points is said to be stable with a particular periodicity depending on the number of points that appear in the Poincare map. And if more points are spread in the Poincare map leading to irregular pattern, it is an indication of chaos / non-periodicity. Bifurcation diagram is the mark for the qualitative changes in system behavior that may occur when the parameters of the system is varied. For numerical computation of bifurcation diagram, the variable (parameter) is increased in a constant step and state variables at the end of the integration are used as the initial values for the next value of the parameter. Our variable parameter in the study of this bifurcation diagrams is the ac voltage.

3.6 Results and discussions

The parametric study is carried out by varying one parameter at a time, while keeping the remaining parameters constant. The variables for this study are ac voltage (V_0), gap-pressure (p_0) and the frequency ratio (r). Dynamic analysis is carried out for the two set of microbeams having the dimensions as given below in the Table 3.2.

Table.3.2 Dimensions of Microbeam under consideration

Parameter	Case-1	Case-2
Width of beam (b) (μm)	80	50
Thickness of beam (t) (μm)	4.5	3
Length of beam (L) (μm)	200	350
Initial air gap (d) (μm)	3	1
Young's modulus E (GPa)	166	169
Poisson's ratio (ν)	0.06	0.06
Density (ρ) (Kg/m^3)	2331	2330
Permittivity of free space (ε_0) (F/m)	8.854×10^{-12}	8.854×10^{-12}

Geometrical dimensions of microbeam greatly influence the dynamic analysis results. Dynamic pull-in voltages vary drastically with the change in length, width, thickness and gap. The other input parameters are choosen randomly. Computer program in MATLAB is developed for solving the non-dimensional equation of motion. The function file providing the second state variable is presented as follows:

```
%%%%%%%%FUNCTION FILE CONTAINING STATE VARIABLE X2%%%%%%%%%%%%%%%%
function y=g2(x1,x2,t)
b=80e-6;L=200e-6;th=4.5e-6;d=3e-6;
A=b*th;
I=b*th^3/12;
E=166e9/(1-0.06^2);rh=2331;
ep=8.8541878e-12;
Vp=86.1;        %DC VOLTAGE to be varied for pull-in prediction
V0=0.5;         %AC VOLTAGE to be varied for intermediate chaos prediction
zi=1e-6;        % VISCOUS DAMPING RATIO
p0=0.2*133.32; % 1 TORR=133.32 Pa, 1 atm=101.325e3 Pa=760 torr
mu=18.3e-6;     %Dynamic viscosity of air
pa=1.01325e5;   %Ambient pressure
L0=65e-9;       %mean free path of air particles
r=0.75;         % non-dimensional parameter
m=rh*A*L;
k=(m)*3.516^2*E*I/(rh*A*L^4);
om0=sqrt(k/m); %NATURAL FREQUENCY
kn=pa*L0/(p0*d*(1-x1));%Knudsen number
mueff=mu/(1+9.638*kn^1.159); %effective visocity
om=r*om0;       %external frequency of AC voltage
A1=b*L;         % AREA
c0=e*A1;
c1=768*mueff*A1^2/pi^6;
c2=(12*A1*om*mueff/(pa*pi^2))^2;
al=c0*(Vp^2+0.5*V0^2)/(2*m*d^3*om0^2);
be=2*c0*V0*Vp/(2*m*d^3*om0^2);
de=0.5*c0*V0^2/(2*m*d^3*om0^2);
term1=2*zi;    %VISCOUS
term2=2*c1*d*(1-x1)/(m*om0*(4*d^4*(1-x1)^4+c2));%SQUEEZE-FILM
term3=term1+term2;
y=-x1-term3*x2+al*(1/(1-x1)^2)+(be/(1-x1)^2)*cos(r*t)
                       +(de/(1-x1)^2)*cos(2*r*t);%-ga*x1^3;
%%%%%%%%%%%%%%%%%%%%%%%%%%%%%%%%%%%%%%%%%%%%%%%%%%%%%%%%%%%%%%%%%%
```

3.6.1 Dynamic pull-in curves

A plot drawn between dc voltage and non-dimensional amplitude at three conditions of ac voltage by setting pressure, frequency ratio as constant. The dynamic pull-in value is identified from the time-history amplitudes at different dc voltages. As this voltage is reached, the amplitude shoots-up and non-dimensional displacement exceed unity, which physically means

that the amplitude exceeds the gap space. The results of the dynamic analysis for two cases considered in Table-3.2 are shown below:

Case1: Here, we varied the amplitude of dc voltage and obtained in each case the time-history and phase trajectory and noted down the amplitude of oscillation. In one of the cases where V_0=10 volts and V_{dc}=70 volts, the following time-history and phase diagram are observed (see Fig.3.3). The time-step maintained in the solver is $h=2\pi/r/1000=0.0126$. It is seen that initially it oscillates with stable center and slowly it tries to escape as seen from the oval shape of phase trajectory.

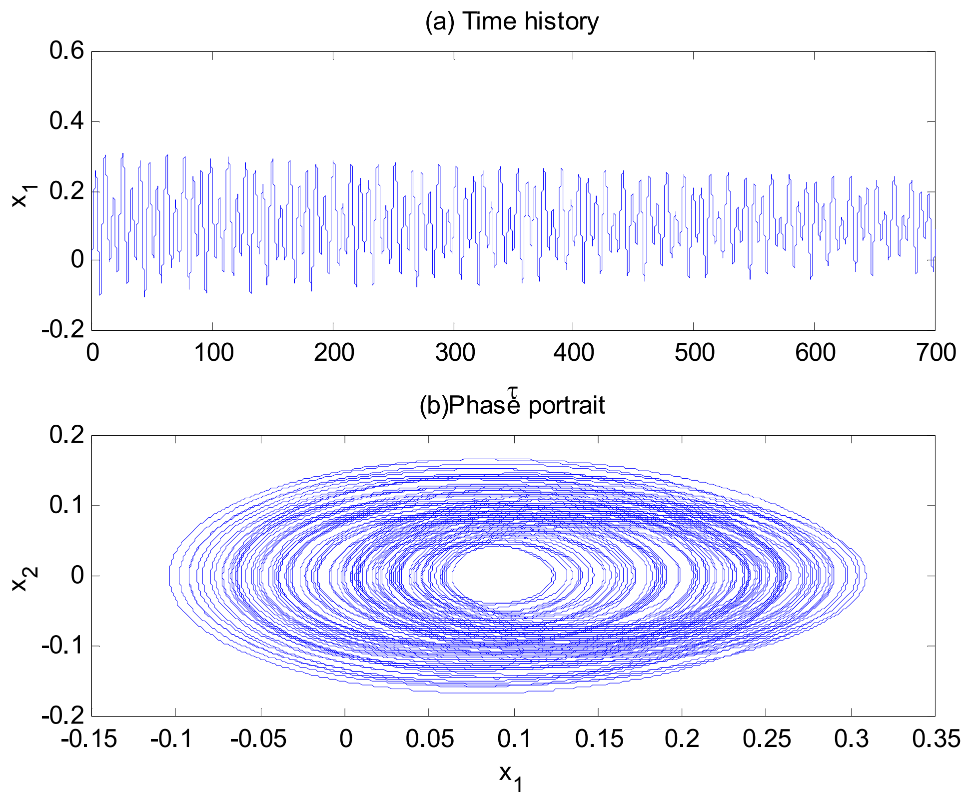

Fig.3.3 Time history and phase plane diagrams for spring mass model at V_{ac}=10v, r=0.5, P_a=800mtorr (1Torr = 133.32Pa).

By calculating the minimum and maximum deflection at particular voltage, in the time history and phase plane diagrams obtained in the Fig.3.3, the amplitude of microbeam can be obtained. The obtained amplitude at various dc voltages are plotted to obtain the dynamic pull-in curves. This dc pull-in voltage predicted is very much important in the design of MEMS devices that

makes use of the microcantilever beams. Only within this limit of dc pull-in voltage, MEMS devices can be operated without failure. So that safety can be ensured at the operating zone of the device in which this microcantilever beams are used. Corresponding to the ac voltages 10v, 20v, and 30v considered in our analysis the dynamic pull-in voltages (dc) are predicted as shown in the Fig.3.4. It is observed that the dynamic pull-in voltage falls with the rise of harmonic ac voltage. That is voltage greatly influences the amplitude of microcantilever beam resonator.

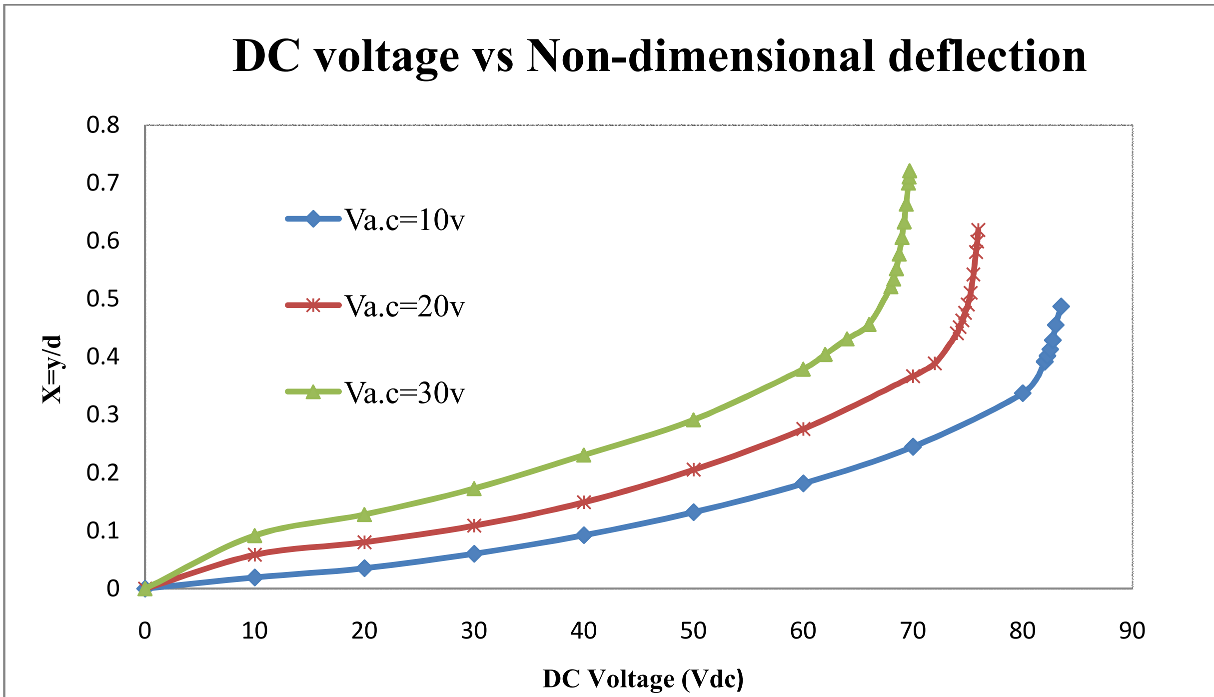

Fig.3.4 dc voltage to amplitude is plotted at different ac voltages with pressure=800mtorr, r=0.5. Pull-in voltages for the three curves are 83.5v, 79.95v, 69.7v

Static pull-in voltage and variation of resonant frequency of microbeam resonator are sometimes of importance. Especially, the resonant frequency of MEMS is a very important parameter as it determinates the amount of force the structure can exert. The resonant frequency indirectly affects design parameters such as quality factor and effects of external noise. The resonant frequency of a MEM structure depends on both the electrostatic force and its deformation and may accordingly demonstrate "spring-softening" or "spring-hardening" effect of the electrostatic force. Fig.3.5 shows the variation of frequency ratio as a function of dc voltage. Here the zero frequency voltage corresponds to each curve is an approximate static pull-in voltage value.

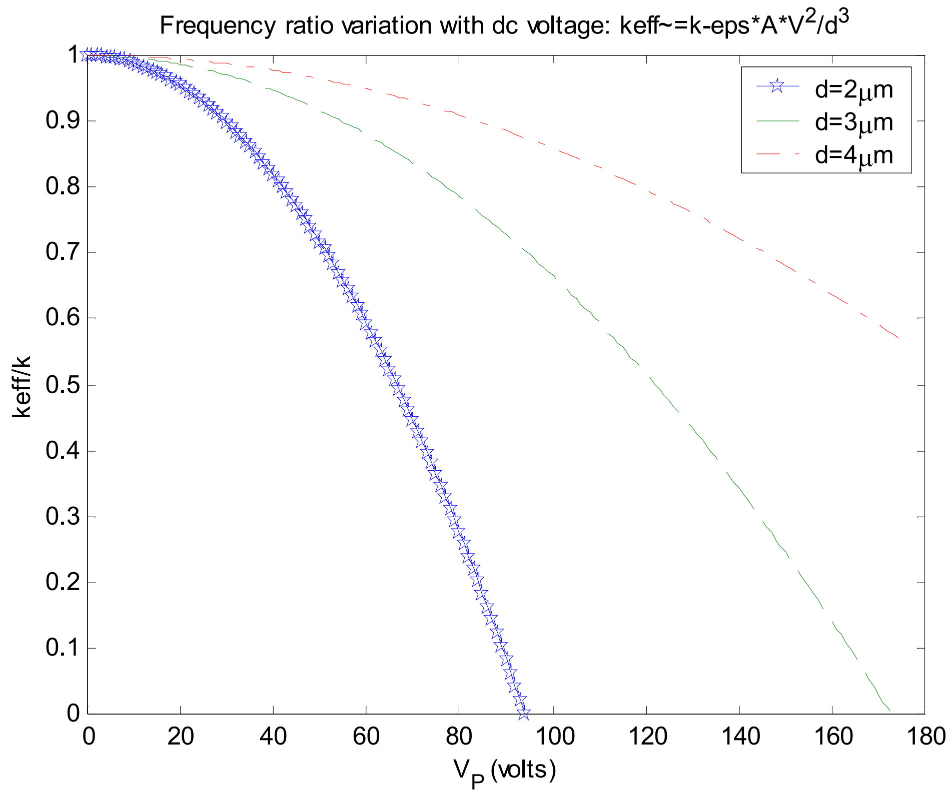

Fig.3.5 Variation of frequency ratio at different gap heights (V_0=0)

It is seen that the resonant frequency increases with the increase of the gap at the same dc bias voltage. The resonant frequency is a monotonically decreasing function of increasing dc bias voltage, when the ac voltage is ignored. More accuracy in frequency results can be obtained from frequency response curves, which includes higher order terms.

Case2: Here again the same dynamic analysis is carried out and the pull-in curves are obtained from the amplitudes of time-histories. Fig.3.6 shows the time history and phase diagram at V_0=0.5 volts and V_P=2.5 volts. It is seen that there is some initial chaos in the system and there after system become periodic. Such a set of time histories and phase plane diagrams are utilized for the calculation of amplitude of microbeam. The difference of maximum to minimum deflection of microbeam under electrostatic actuation gives the amplitude at that particular voltage. Here the minimum and maximum of x_1 gives the amplitude at the voltage that we considered. Fig.3.7 shows the Poincare map at this configuration, where 54 points have been converged into only 9 points showing overall periodicity of the system.

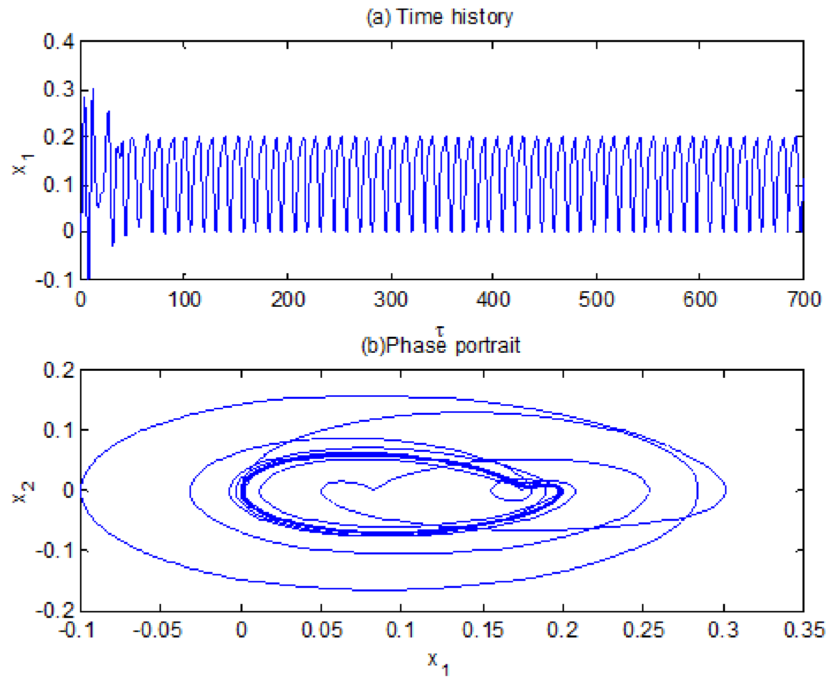

Fig.3.6 Time history and phase plane diagrams for spring mass model at V_{ac}=0.5v, r=0.5, P_a=800mtorr (1Torr = 133.32Pa)

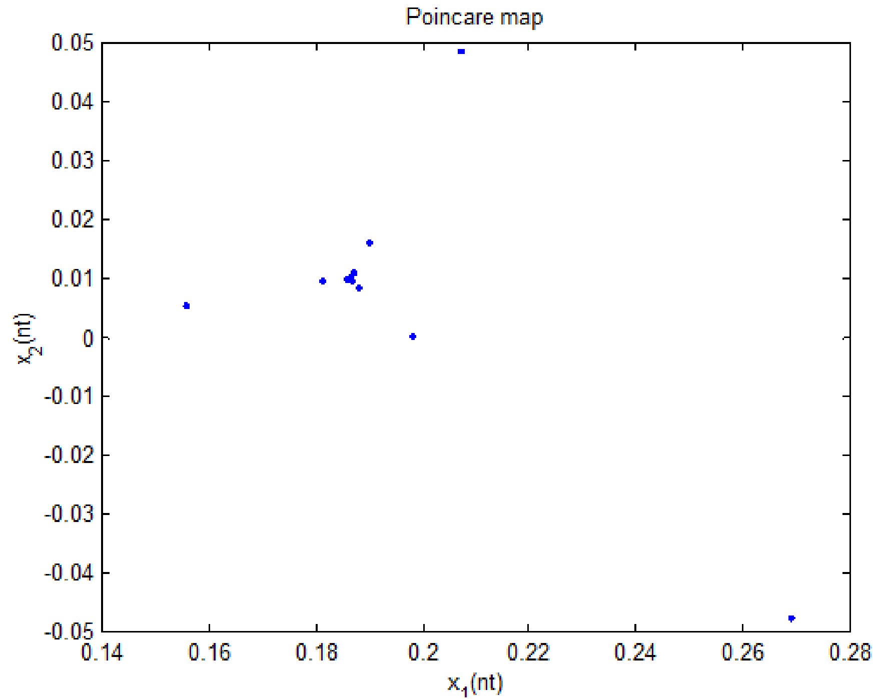

Fig.3.7 Poincare map at V_0=0.5 v and V_P=2.5 volts

Fig.3.8 shows the pull-in curves obtained for three different ac voltage amplitudes.

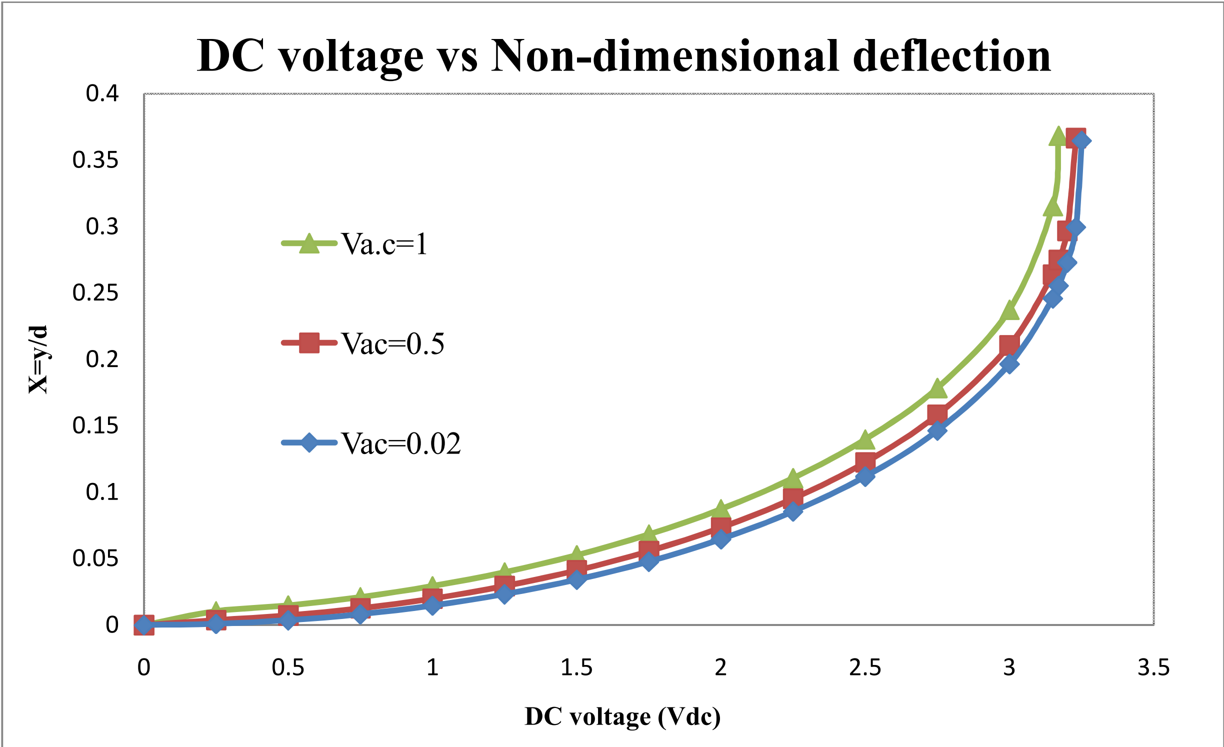

Fig.3.8 dc voltage to amplitude is plotted at different ac voltages with pressure=800mtorr, r=0.5. Pull-in voltages for the three curves are 3.25v, 3.23v, 3.17v.

With the increase of ac voltage the corresponding dynamic pull-in voltage falls. And hence we can notice that high ac voltage minimize the region of stability. For a device to be operated, there are many parameters to be considered. Based on the requirements and the application at which the device is used these data obtained from pull-in curves are utilized in order to evaluate whether the system can be operated effectively without any failure or not.

3.6.2 Frequency response with pressure variation

Case1: The squeeze-film pressure effect in terms of gap pressure p_o is studied. As shown in Fig.3.9, at different operating pressures the response curve amplitudes are changing. The system behavior is examined with the help of frequency response plots that are plotted between the frequency ratio and the amplitudes of non-dimensional deflection. These curves are also obtained from the time-history plots.

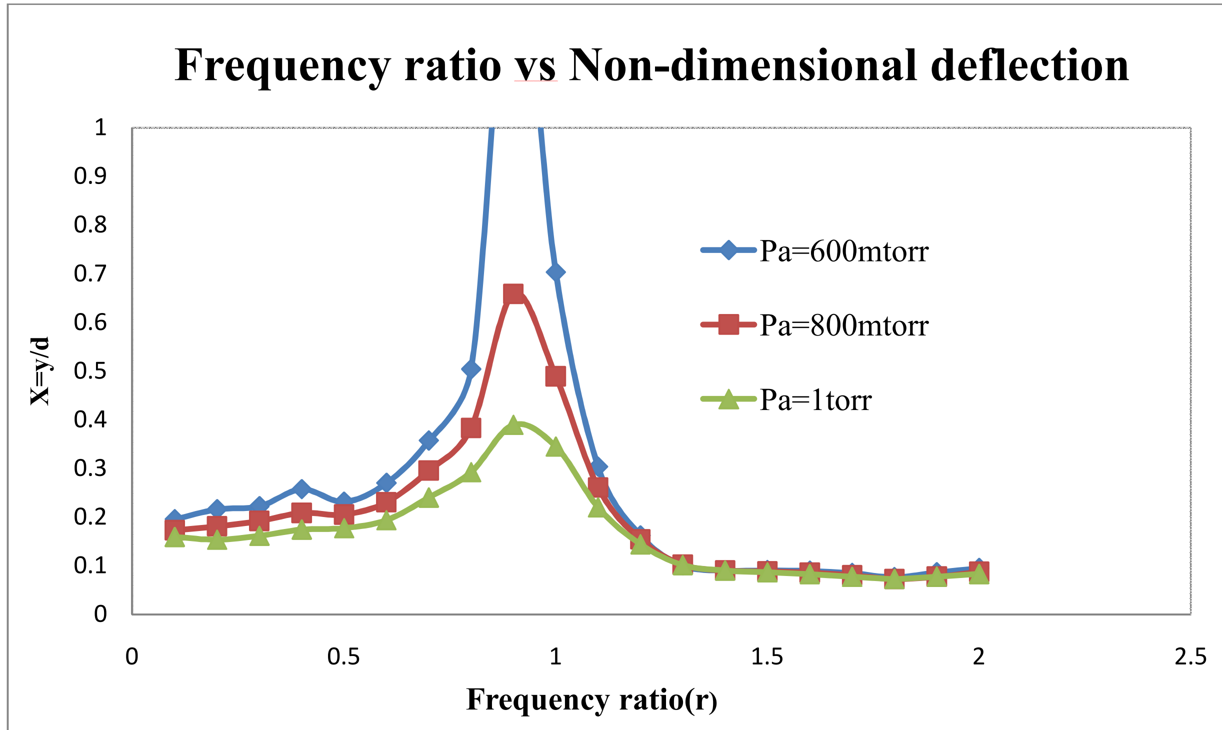

Fig.3.9 Frequency ratio vs Non-dimensional deflection for spring-mass model at V_{ac}=20v, V_{dc}=50v.

With the rise of pressure it is found that the amplitude falls due to the fact that the damping becomes prominent at high pressures. Hence the peak of frequency response curve falls as pressure increases. These plot is for the first case of dimension considered.

Case2: For the second case also, a similar analysis is carried out and the effect of frequency ratio on the amplitudes of response is predicted. Fig. 3.10 shows the corresponding frequency response curve. Based on the dimensions of microbeam the operating pressure varies. Hence before design the dynamic analysis is carried out for finding the operating parameter of the device. Different microbeams have different operating regions due to the variation in dimensions. Our study of these frequency response plots corresponding to system parameters such as pressure indicate the stable operation region of device to be operated at a particular environment. The frequency response is also obtained directly from FFT analysis and one can analyze the curves to known the dynamic stability of the system at corresponding operating pressures.

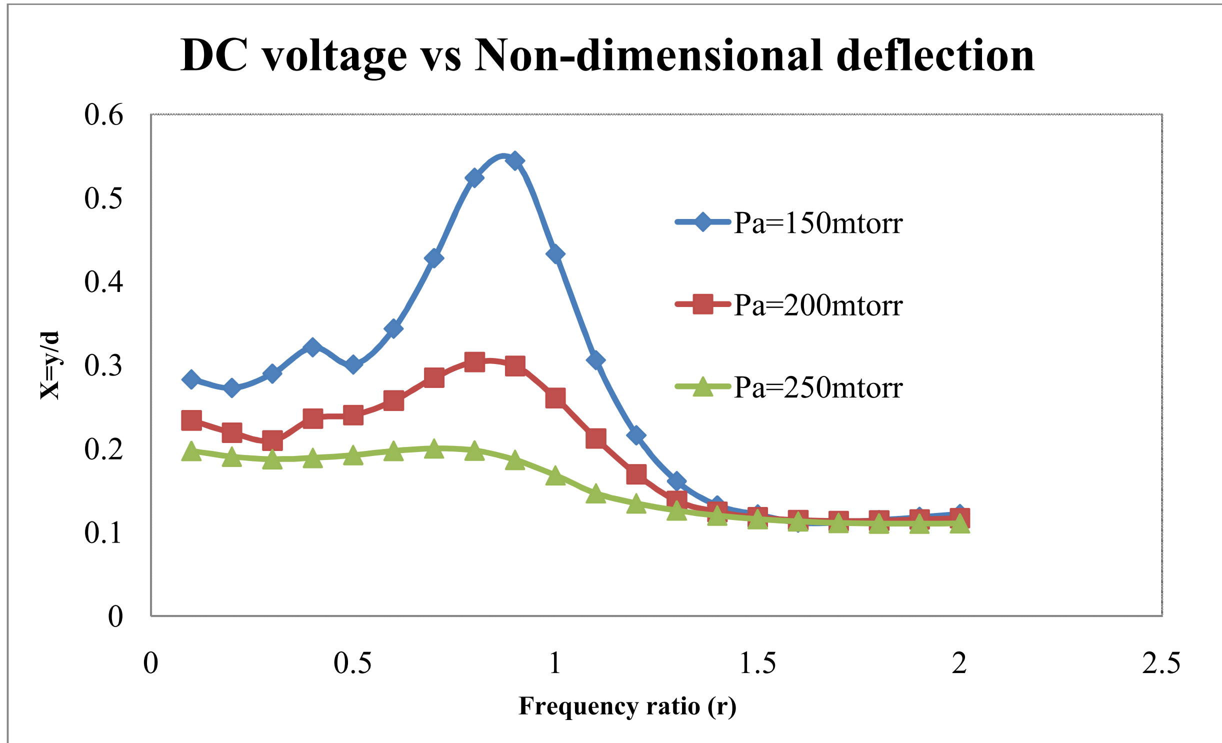

Fig.3.10 Frequency ratio vs Non-dimensional deflection for spring-mass model at V_{ac}=1v, V_{dc}=2v.

3.6.3 Frequency response with ac voltage variation

Case 1: Frequency response curves are then obtained by varying the ac voltage amplitudes at constant pressure condition of p_0=800 milli-torr. Fig.3.11 shows these frequency domain plots. It is observed that with the increase of ac voltage the amplitude of microbeam increases. And another observation is that the peak of frequency response curve rises with the rise in ac voltage that is applied between the microbeam and the fixed substrate.

Case 2:

Fig 3.12 shows the system behavior at different ac voltages. With the increase of ac voltage the peak of frequency response curve rises. High amplitude is obtained corresponding to high input ac voltage that is given to the microcantilever beam system.

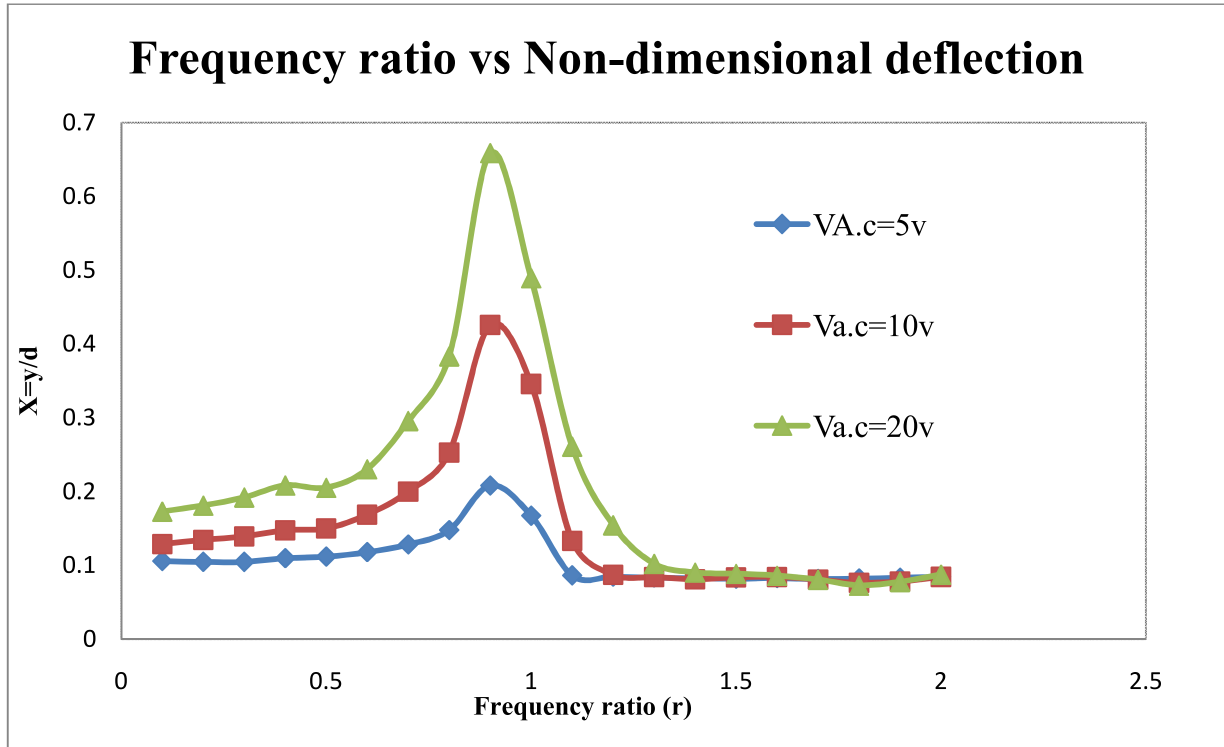

Fig.3.11 Frequency ratio vs Non-dimensional deflection for spring-mass model at V_{dc}=50v, pressure p_0=800mtorr.

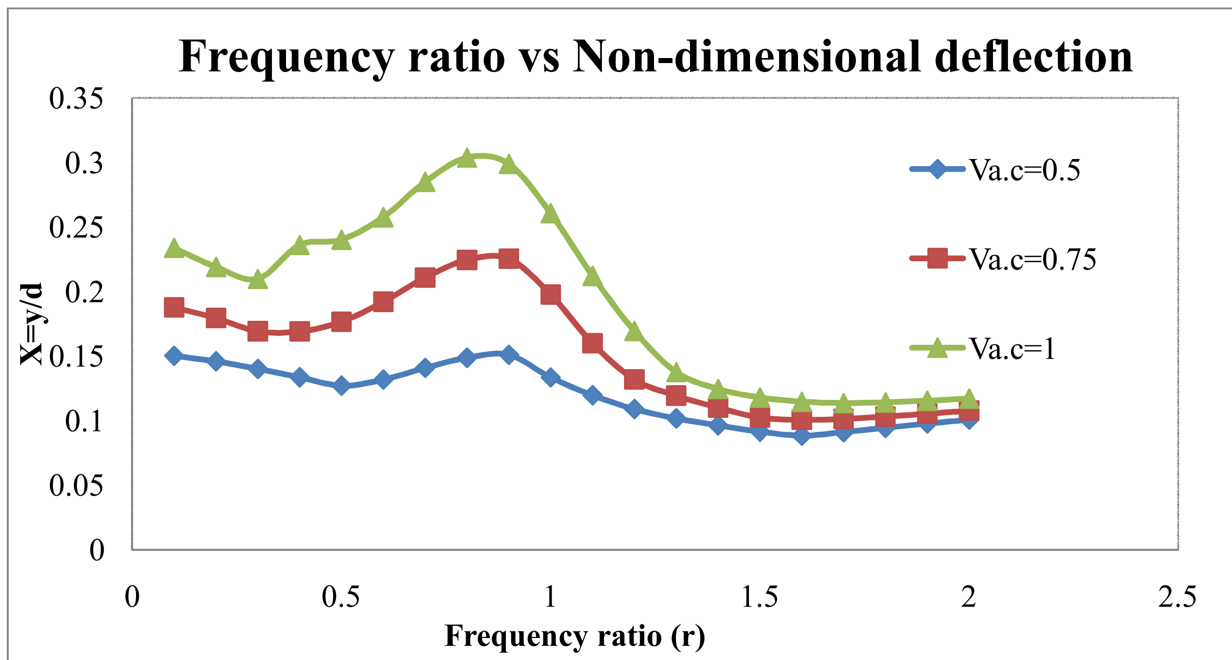

Fig.3.12 Frequency ratio vs Non-dimensional deflection for spring-mass model at V_{dc}=2v, pressure p_0=800mtorr.

CHAPTER-4

4. DISTRIBUTED PARAMETER MODELS

The dynamics of MEMS microcantilever beams are represented by partial-differential equations (PDEs) and associated boundary conditions. The most widely adopted method to treat these distributed-parameter problems is to reduce them to ordinary-differential equations (ODEs) in time, using the Galerkin reduced-order technique. Hence the reduced-order modeling of MEMS is gaining attention as a way to balance the need for enough fidelity in the model against the numerical efficiency necessary to make the model of practical use in MEMS design.

The formulated reduced order equations are then solved numerically using the fourth-order Runge-Kutta numerical technique in the MATLAB. This reduced-order model is utilized to investigate the non-linear dynamics of microcantilever beam.

4.1 Mathematical formulation of equation of motion

A precise prediction of the pull-in plays an important role in the device operations. The prediction of pull-in started herein by establishing the governing distributed equations of motion for the deformable micricantilever beam as shown in Fig.4.1. The formulated equation is given by:

$$E'I\frac{\partial^4 w}{\partial x^4} + \rho bh\frac{\partial^2 w}{\partial t^2} + c\frac{\partial w}{\partial t} - N\frac{\partial^2 w}{\partial x^2} = F_E - F_A \tag{4.1}$$

Where,

$$E' = \frac{E}{(1-\nu^2)}$$

Here E' is the effective Young's modulus, $A=bt$ and $I = \frac{bt^3}{12}$

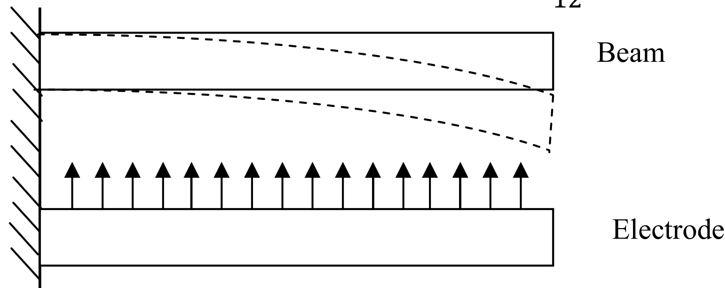

Fig.4.1. Microbeam oscillator

The axial force $N=\sigma bh$ can be taken as zero for the cantilever beam as there is no residual stress in it. The electrostatic force per unit length developed by the electrostatic actuation is given by:

$$F_E = \frac{\epsilon_0 V^2 b}{2(d-w)^2} \tag{4.2}$$

F_E represents the equivalent pressure on the deformed plate due to the applied electrostatic force developed per unit beam length.

Here,

$V = [V_P + V_o cos\ (\omega t)]$.

In order to model squeeze-film damping force F_A, following are considered:

The two dimensional Reynolds equation for the fluid flow is given by:

$$\frac{\partial}{\partial x}\left(\frac{\rho_a g^3}{12\mu_{eff}}\frac{\partial p}{\partial x}\right) + \frac{\partial}{\partial y}\left(\frac{\rho_a g^3}{12\mu_{eff}}\frac{\partial p}{\partial y}\right) = \frac{\partial(\rho_a g)}{\partial t} \tag{4.3}$$

where μ, p, ρ_a and g represents the effective air viscosity, pressure, air density, and air-film thickness respectively.

The effective air viscosity 'μ_{eff}' is obtained similar to that in a SDOF model, using Veijola's theory. That is:

$$\mu_{eff} = \frac{\mu_0}{(1 + 9.638{K_n}^{1.159})} \tag{4.4}$$

Intermolecular collisions play a prominent role and the flow properties will affect the Knudsen number 'K_n', which is a dimensionless measure of the relative magnitudes of the gas mean free path and flow characteristic length. One of the most widely used applications for the Knudsen number is in microfluidics and MEMS device design. We adopted

$$K_n = \frac{\lambda}{g} \tag{4.5}$$

where K_n is Knudsen number, λ=0.064μm and g = (d-w).

Assuming the gap is much less than the beam length, i.e. g<<L, one can obtain the equivalent pressure force per unit beam length due to the squeeze-film effect as follows:[see Krylov and

Maimon, 'Pull-in dynamics of elastic beam actuated by continuously distributed electrostatic force' J. Vib. Acoust, Vol.126, pp.332-342, 2004]

$$F_A = -K_B \frac{\partial \hat{g}}{\partial t} \tag{4.6}$$

where,

$$\hat{g} = \frac{g}{d}, K_B = \frac{3\mu\hat{b}^2}{2\hat{g}^3}, \hat{b} = \frac{B}{d} \tag{4.7}$$

In common practice, since B >> g, K_B could be large enough such that F_A is too large to neglect in the governing equation (4.1) as compared to electrostatic force term F_E.

For the convenience of ensuring analysis, the system equation (4.1) is further non-dimensionalized to be of the form

$$\frac{\partial^4 \hat{w}}{\partial \hat{x}^4} + \frac{\partial^2 \hat{w}}{\partial \tau^2} + \left(\hat{c} + \hat{K}_B\right)\frac{\partial \hat{w}}{\partial \tau} = \alpha \hat{F}_E \tag{4.8}$$

Where

$$\hat{w} = \frac{w}{d}, \hat{x} = \frac{x}{L}, \tau = \frac{t}{T}, \hat{b} = \frac{b}{d} \tag{4.9}$$

$$T = \sqrt{\frac{\rho A L^4}{EI}}, \hat{c} = \frac{cL^4}{EIT}, \hat{F}_E = \frac{V^2}{(1-\hat{w})^2} \tag{4.10}$$

$$\alpha = \frac{\varepsilon_o b L^4}{2EId^3}, \hat{\mu} = \frac{L^4}{EIT}\mu, \hat{K}_B = \frac{\hat{\mu}\hat{b}^3}{(1-\hat{w})^3} \tag{4.11}$$

In equation (4.8), the beam width $\hat{b}$ affects the squeeze-film effect through the term associated with $\hat{K}_B$. With a complete system equation in hand, model decomposition is performed to derive the pull-in voltages.

4.2 Normalization procedure

The method of Galerkin decomposition is employed herein to approximate the system equation (4.8). So the equation (4.8) can be reduced to an ordinary differential equation in terms

of the first-order approximations of the model shape function. The deflection of the beam can be approximated as:

$$\widehat{w}(\hat{x},\tau) = \sum_{n=1}^{M} \phi_n(\hat{x}) q_n(\tau) \tag{4.12}$$

where $\phi_n(\hat{x})$ is n^th^ cantilever beam mode shape, no and $q_n(\tau)$ is n^th^ generalized coordinate. M is number of modes considered. Thus it results-in M ordinary 2nd order differential equations in terms of q_n, n=1, 2, 3. . . M.

$$\phi(\hat{x}) = \frac{1}{N_2}[(\sin\beta LX - \sinh\beta LX) - N_1(\cos\beta LX - \cosh\beta LX)] \quad \text{for cantilever} \tag{4.13}$$

Where,

$$N1 = \frac{\sin\beta L + \sinh\beta L}{\cos\beta L + \cosh\beta L} \tag{4.14}$$

$$N_2 = (\sin\beta L - \sinh\beta L) - N_1(\cos\beta L - \cosh\beta L) \tag{4.15}$$

where $\beta L = 1.875$ for first mode of cantilever beam. In present case one term (mode) approximate is considered. i.e. $\widehat{w} = \phi_1(\hat{x})q_1(\tau) = \phi_1(X)q_1(\tau)$

$\phi(X)$ Is chosen for normalization such that,

$$\int_0^1 \phi^2\, dx = 1 \tag{4.16}$$

By using the Taylor series of expansion, the equation (4.8) is expanded up to four terms. The expanded equation is simplified as:

$$\frac{\partial^4\widehat{w}}{\partial\hat{x}^4} + \frac{\partial^2\widehat{w}}{\partial\tau^2} + \left[\hat{c} + \hat{\mu}\hat{b}^3(1 + 3\widehat{w} + 6\widehat{w}^2 + 10\widehat{w}^3 + 15\widehat{w}^4)\right]\frac{\partial\widehat{w}}{\partial\tau}$$

$$= \alpha V^2(1 + 2\widehat{w} + 3\widehat{w}^2 + 4\widehat{w}^3 + 5\widehat{w}^4) \tag{4.17}$$

We know that,

$$\widehat{w} = \phi(\hat{x})q(\tau) \tag{4.18}$$

So,

$$\Longrightarrow \frac{\partial^4 \widehat{w}}{\partial x^4} = q\frac{\partial^4 \phi}{\partial x^4} = q(\beta L)^4 \phi = q{\omega_1}^2 \phi$$

$$\Longrightarrow \frac{\partial^4 \widehat{w}}{\partial x^4} = q{\omega_1}^2 \phi \tag{4.19}$$

Also

$$\frac{\partial^2 \widehat{w}}{\partial \tau^2} = q^{''} \phi \tag{4.20}$$

$$\frac{\partial \widehat{w}}{\partial \tau} = q^{'} \phi \tag{4.21}$$

4.3 Reduced order model

By substituting the equations (4.19-4.21) in the equation (4.17) we obtain:

$$q{\omega_1}^2 \phi + q^{''} \phi + \left[c + \hat{\mu}\hat{b}^3(1 + 3\phi q + 6\phi^2 q^2 + 10\phi^3 q^3 + 15\phi^4 q^4)\right] q^{'} \phi$$
$$= \alpha V^2 (1 + 2\phi q + 3\phi^2 q^2 + 4\phi^3 q^3 + 5\phi^4 q^4) \tag{4.22}$$

Integrating both sides with respect to '$\hat{x}$' after multiplying by 'ϕ' hence the equation is as follows:

$$\int_0^1 \left\{q{\omega_1}^2 \phi^2 + q'' \phi^2 + \left[c + \hat{\mu}\hat{b}^3(1 + 3\phi q + 6\phi^2 q^2 + 10\phi^3 q^3 + 15\phi^4 q^4)\right] q' \phi^2\right\} dx$$

$$= \int_0^1 [\alpha V^2 (\phi + 2\phi^2 q + 3\phi^3 q^2 + 4\phi^4 q^3 + 5\phi^5 q^4)]\, d\hat{x} \tag{4.23}$$

on simplification the equation (4.23) with equations(4.19-4.21), we get:

$$q'' + \left[\left(c + \hat{\mu}\hat{b}^3\right) + 3\hat{\mu}\hat{b}^3 q \int_0^1 \phi^3 dx + 6\hat{\mu}\hat{b}^3 q^2 \int_0^1 \phi^4 dx + 10\hat{\mu}\hat{b}^3 \int_0^1 \phi^5 dx + 15\hat{\mu}\hat{b}^3 \int_0^1 \phi^6 dx\right] q'$$

$$+q{\omega_1}^2 = \alpha V^2 \left[\int_0^1 \phi dx + 2q + 3\,q^2 \int_0^1 \phi^3 dx + 4q^3 \int_0^1 \phi^4 dx + 5q^4 \int_0^1 \phi^5 dx \right] \tag{4.24}$$

Using the state variables x_1, x_2 the equation 4.24 can be written as:

$$\Rightarrow \dot{x}_2 = -\left[c + \hat{\mu}\hat{b}^3(1 + 3x_1 t_2 + 6{x_1}^2 t_1 + 10{x_1}^3 t_0 + 15{x_1}^4 t_{00})\right]x_2 - [(\beta L)^4 - 2\alpha V^2]x_1 + \alpha V^2(t_4 + 3{x_1}^2 t_2 + 4{x_1}^3 t_1 + 5{x_1}^4 t_0 \tag{4.25}$$

Here,

$$q = x_1 \tag{4.26}$$

$$q' = x_1' = x_2 \tag{4.27}$$

$$q'' = x_1'' = \dot{x}_2 \tag{4.28}$$

also

$$t_{00} = \int_0^1 \phi^6 dx\,, t_0 = \int_0^1 \phi^5 dx\,,\ t_1 = \int_0^1 \phi^4 dx\,,\ t_2 = \int_0^1 \phi^3 dx\,,\ t_3 = \int_0^1 \phi^2 dx = 1 \tag{4.29}$$

The obtained results can be utilized to study the behavior of present electrostatic cantilever resonators and capacitive resonators.

Based on above analysis, programs are developed in MATLAB to predict the integrals of the mode shape function and define the state variable functions in order to solve the equation (4.25). Following function program shows the integration procedure during calculation of static and dynamic pull-in states.

```
%%%%%%%%%%%%%%%%%%%%%%%%%%%
syms x phi;
mu=(sin(1.875104)+sinh(1.875104))/(cos(1.875104)+cosh(1.875104));
y=0:0.01:1;
bl=1.875104;
n2=sin(1.875104)-sinh(1.875104)-mu*(cos(1.875104)-cosh(1.875104));
t5=((sin(1.875104.*y)-sinh(1.875104.*y)-mu.*(cos(1.875104.*y)-
cosh(1.875104.*y))))/n2;;
ma=max(t5);
phi=(sin(1.875104*x)-sinh(1.875104*x)-mu*(cos(1.875104*x)-
cosh(1.875104*x)))/n2;
```

```
t3=eval(int(phi^2,0,1));
t2=eval(int(phi^3,0,1))/t3;
t4=eval(int(phi,0,1))/t3
t1=eval(int(phi^4,0,1))/t3;
t3=1;
eps=8.854e-12;
b=8e-6;t=2e-6;
L=100e-6;
E=166e9;%/(1-0.06^2);
I=b*t^3/12;
d=0.5e-6;
alpha=eps*b*L^4/(2*E*I*d^3);
q=0:0.01:1;
vdc=sqrt((1.875104)^4*(t1.*q.^3-2*t2.*q.^2+t3.*q)/(alpha*t4));
vp=max(vdc);
figure(1);
plot(vdc,q);
st1=3*E*I/L^3;
%FIRST PULL-IN VALUE IS ESTIMATED FROM ONE-MODE GALERKIN APPROACH AND USING
THIS STIFFNESS IS COMPUTED WITH ASSUMPTION THAT PULL-IN OCCURS AT 1/3RD OF
INITIAL GAP
st=27*vp^2*eps*b*t/(8*d^3);
vdc1=sqrt(2*d^3.*(1-y).^2.*y*st/(eps*b*t));% IDEAL CURVE
figure(2)
plot(vdc,y,vdc1,y);
%%%%%%%%%%%%%%%%%%%%%%%%%%%%%%%%
```

4.4 Results and discussions

Case1: Static pull-in behaviour can be studied by avoiding first two terms in eq.(4.24). Fig.4.2 shows the pull-in curve obtained from one-mode approximation using Galerkin's method in comparison with the theoretical pull-in curve. It is seen that the non-dimensional gap height w/d at which pull-in occurs is at round 0.46 in comparison to 0.33 for the theoretical approach. This agrees well with the literature available. The dynamic equations (4.24) are solved again using R-K solver with following sub-function:

```
%%%%%%%%%%%%%%%%%%%%%%%%%%%%%%%%%%%%%%%%%%%%%

function y=ji(x1,x2,t,Vp)
to=0.4876; t1=0.5872;t2=0.7389;t3=1;t4=1.566;too=0.4171;
eps=8.854e-12;
l=350e-6;b=50e-6;th=3e-6;d=1e-6;
ro=2330;E=169e9/(1-0.06^2);
bm=b/d;
A=b*th; I=b*th^3/12;
Vo=0.02;     %AC VOLTAGE
alpha=eps*b*l^4/(2*E*I*d^3);
r=1;
% DAMPING COEFFICIENT FROM NON-DIMENSIONAL PARAMETER
```

```
mu=18.6*10^-6;
pa=0.8*133.32;
kn=0.0064/(pa*d);
mueff=mu/(1+9.638*kn^1.159);
wo=(1.875)^2*sqrt((E*I)/(ro*A*l^4));
MU=(mueff*l^4*wo)/(E*I);
c=0.73; % non dimensional damping quotient;
B=1.875104;
V=Vp+Vo*cos(r*t);
Z=MU*bm^3;
y=-(c+Z*(1+3*x1*t2+6*x1^2*t1+10*x1^3*to+15*x1^4*too))*x2-(B^4-
2*alpha*V^2)*x1+alpha*V^2*(t4+3*x1^2*t2+4*x1^3*t1+5*x1^4*to);

%%%%%%%%%%%%%%%%%%%%%%%%%%%%%%%%%%%%%%%%%%%%%%
```

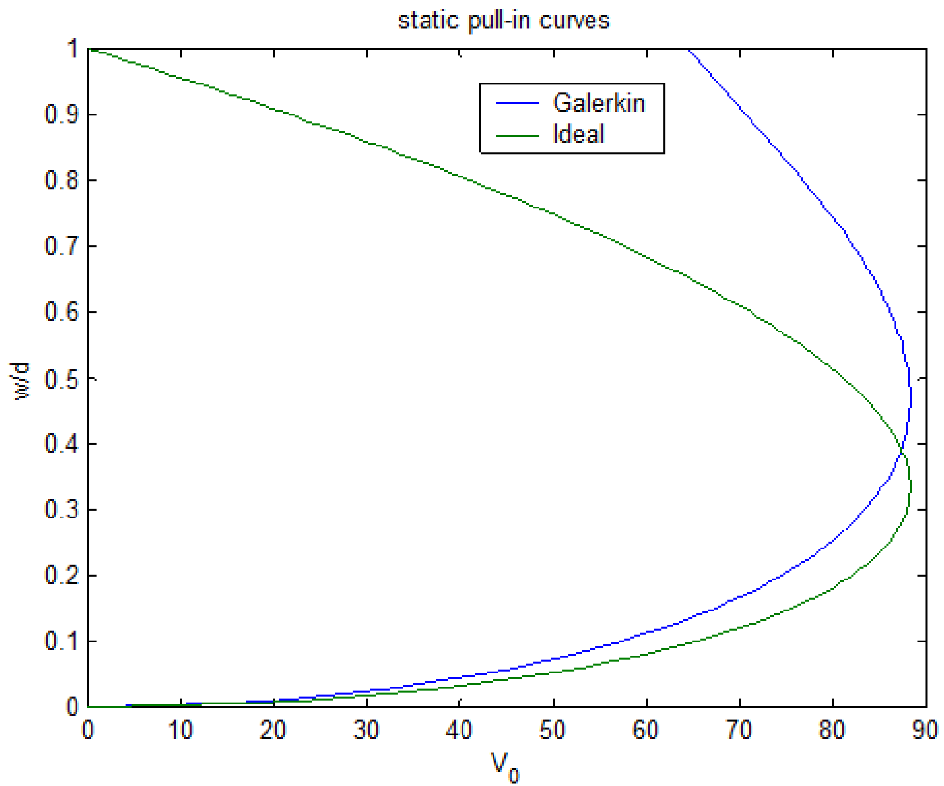

Fig. 4.2 Static pull-in for case-1

By varying the dc voltage V_P, we can obtain again a non-dimensional amplitude plots representing the dynamic pull-in curves. Fig.4.3 shows the time-history and phase diagram at V_P=79.25 volts and V_0=10 volts, where system is at the verge of pull-in state.

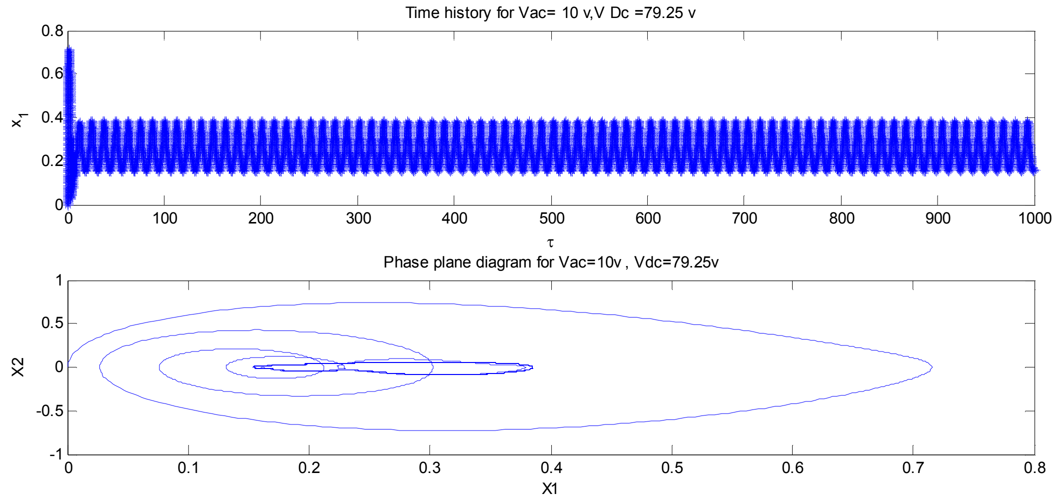

Fig.4.3 Time history and phase plane diagrams for reduced–order Galerkin model at V_{ac}=10v, r=0.5, P_a=800mtorr (1Torr = 133.32Pa)

By calculating the minimum and maximum deflection at particular voltage, in the time history and phase plane diagrams, the amplitude of microbeam can be obtained. The amplitude at different dc voltages is calculated and a plot is drawn between the dc voltage and the non-dimensional deflection as shown in Fig.4.4.

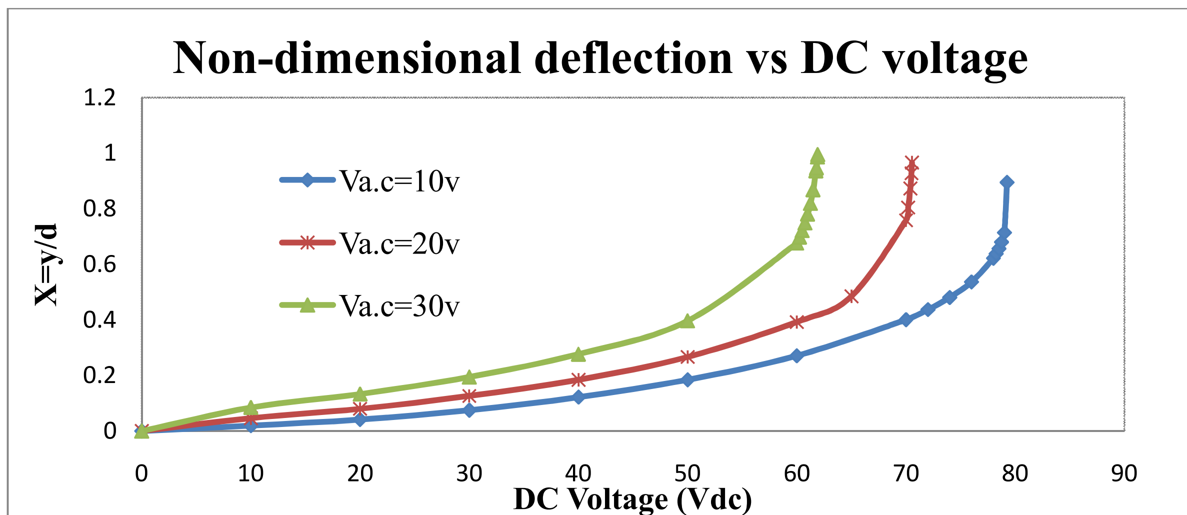

Fig.4.4 dc voltage to amplitude is plotted at different ac voltages with pressure=800mtorr, r=0.5. Pull-in voltages for the three curves are 79.25v, 70.55v, 61.92v.

These curves are at three different ac voltages. It is shown that with the rise of ac voltage applied the dynamic pull-in voltage falls.

Case2: A similar approach is adopted for the second set of geometry and it is found that the dynamic pull-in voltage for V_0=0.5 volts occurs at 2.75 volts. By calculating the minimum and maximum deflection at particular voltage, in the time history and phase plane diagrams as obtained in the Fig.4.5, the pull-in curve can be plotted as shown in Fig.4.4.

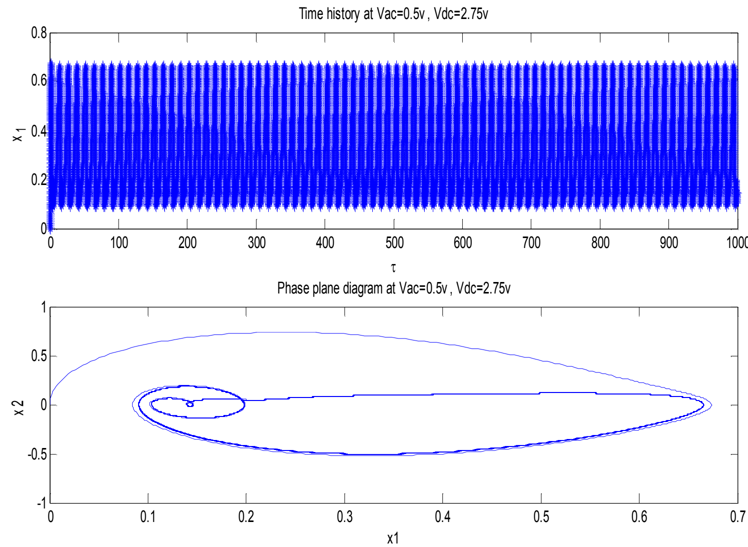

Fig.4.5 Time history and phase plane diagrams for reduced–order Galerkin model at V_{ac}=0.5v and V_{dc}=2.75v, r=0.5, P_a=800mtorr (1Torr = 133.32Pa)

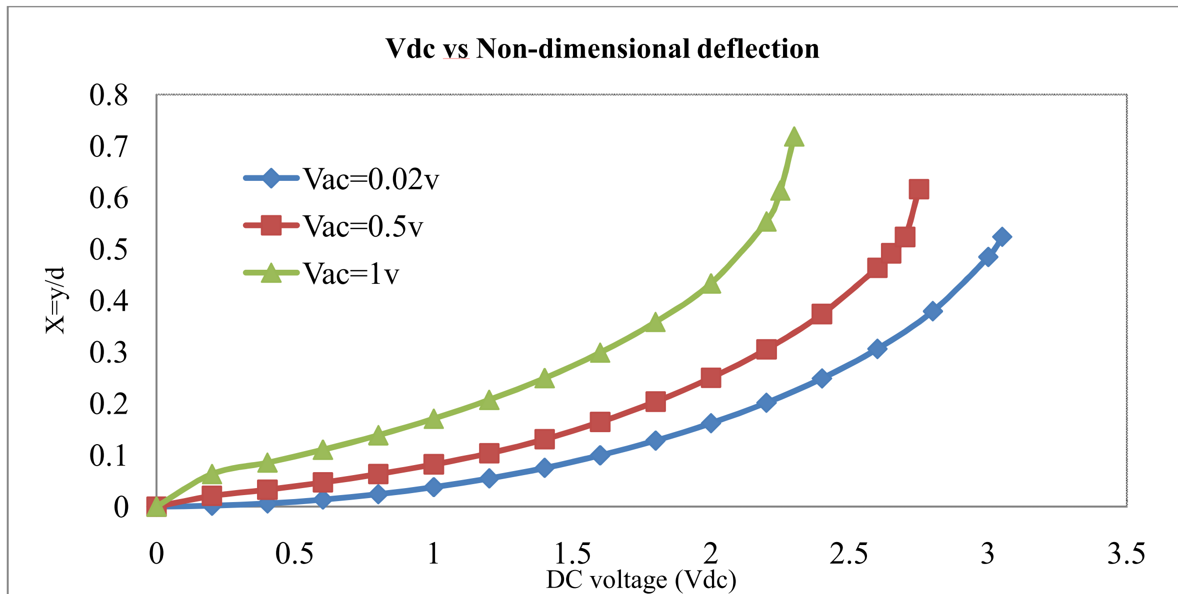

Fig.4.6 Dynamic pull-in curves at three different ac voltages with pressure=800mtorr, r=0.5. Pull-in voltages for the three curves are 3.25v, 3.23v, 3.17v

Dynamic pull-in curves as shown in the Fig.4.6 indicate the pull-in voltages at three different ac voltages. It is shown that with the rise of ac voltage applied the dynamic pull-in voltage falls. The pull-in voltage is the primary and essential analysis to be carried out for the prediction of stability for the MEMS microbeams. The zone of stability predicted can be made use for the design of these MEMS devices with makes use of this microbeams. Fig.4.6 shows the frequency response diagram for case-1 at a pressure p_0=600 mtorr.

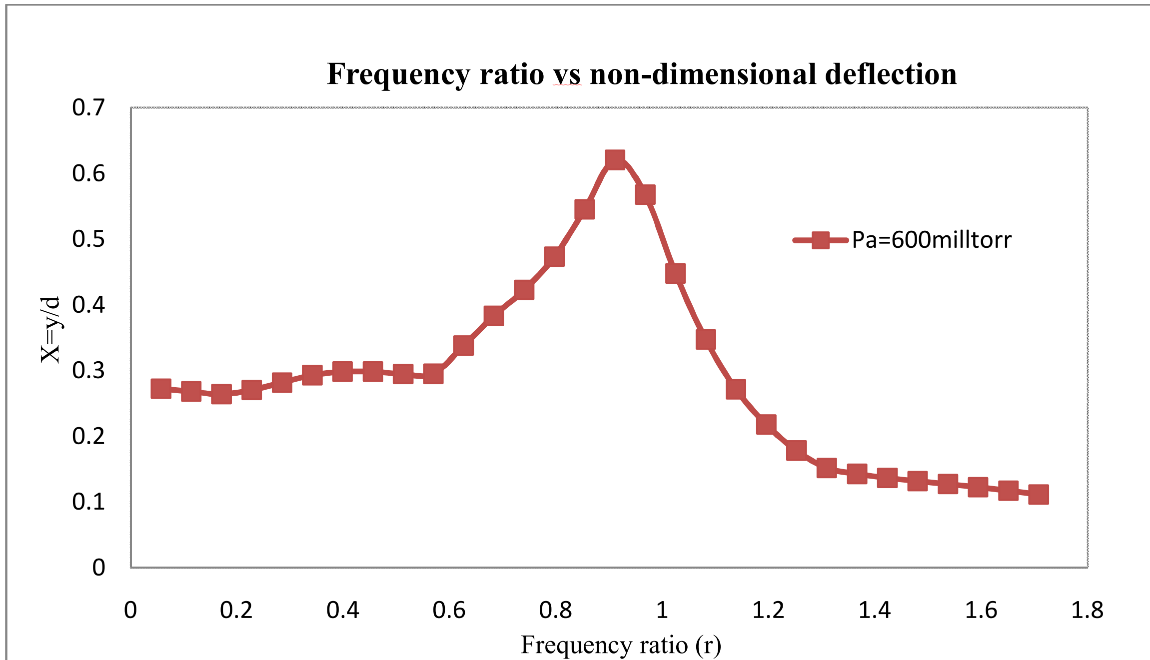

Fig.4.7 Frequency ratio vs Non-dimensional deflection for reduced-order Galerkin model at V_{ac}=20v , V_{dc}=50v

Frequency response curves are drawn with the variation of system input parameters such as ac voltage and the pressure. As indicated in the Fig.4.7, with the increase of ambient pressure the peak of the frequency response falls due to the increased damping effect which opposes the deflection of the microbeam. With the variation of the pressures, it is observed that the curves deviated very slightly. Fig.4.8 shows the frequency response curve for the second case under consideration at a gap pressure p_0=150 mtorr. It is seen from the figure that pull-in amplitude occurs at this pressure due to very small damping effect before it reaches primary resonant zone r=1. The figure shows the softening nonlinearity in the system with bent of backbone curve backwards. Fig.4.9 shows the effect of variation of ac voltage amplitude on frequency response for case-1. It is seen that with increase of ac volage the peak values are increasing.

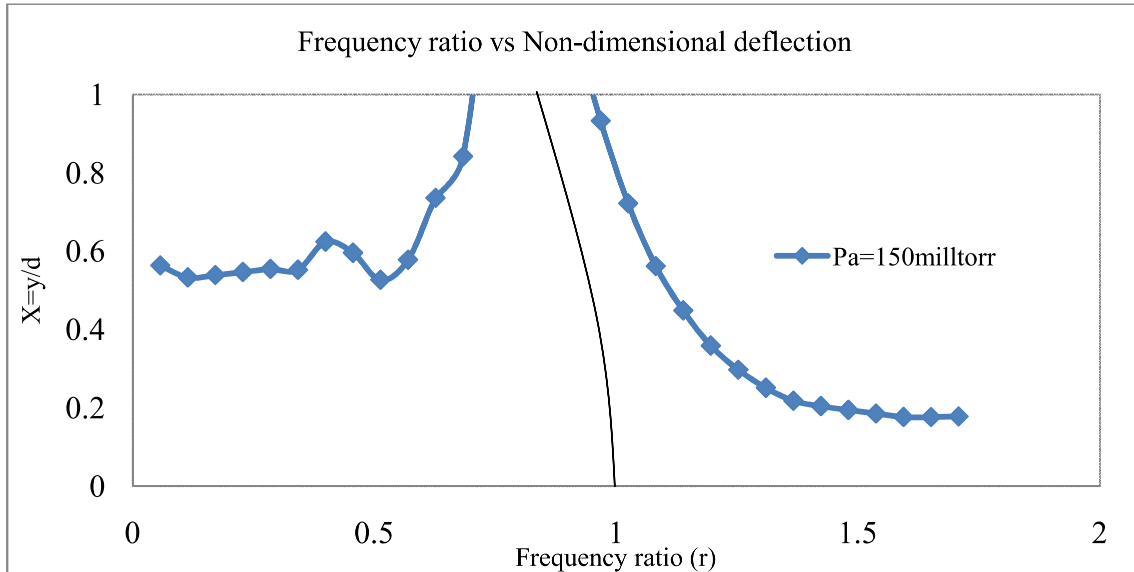

Fig.4.8 Frequency ratio vs Non-dimensional deflection for reduced-order Galerkin model at V_{ac}=1v , V_{dc}=2v.

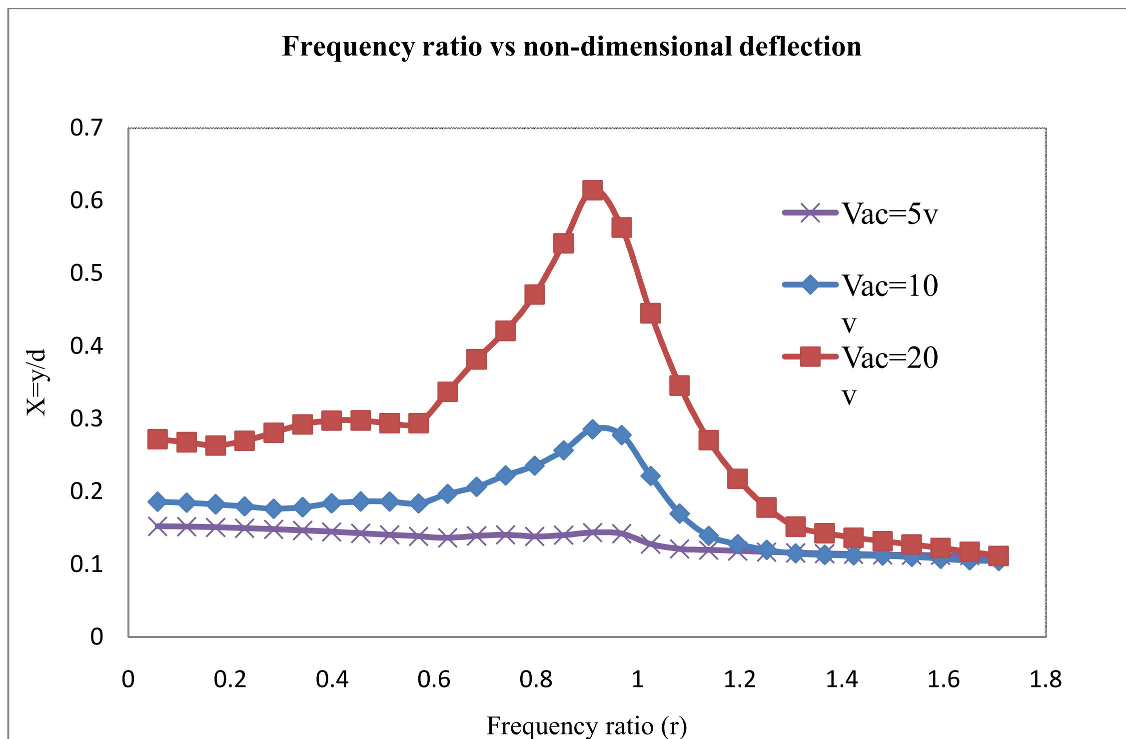

Fig.4.9 Frequency ratio vs Non-dimensional deflection for reduced-order Galerkin model at V_{dc}=50v, pressure =800mtorr.

A similar frequency response plot is drawn for case-2 as shown in Fig.4.10.

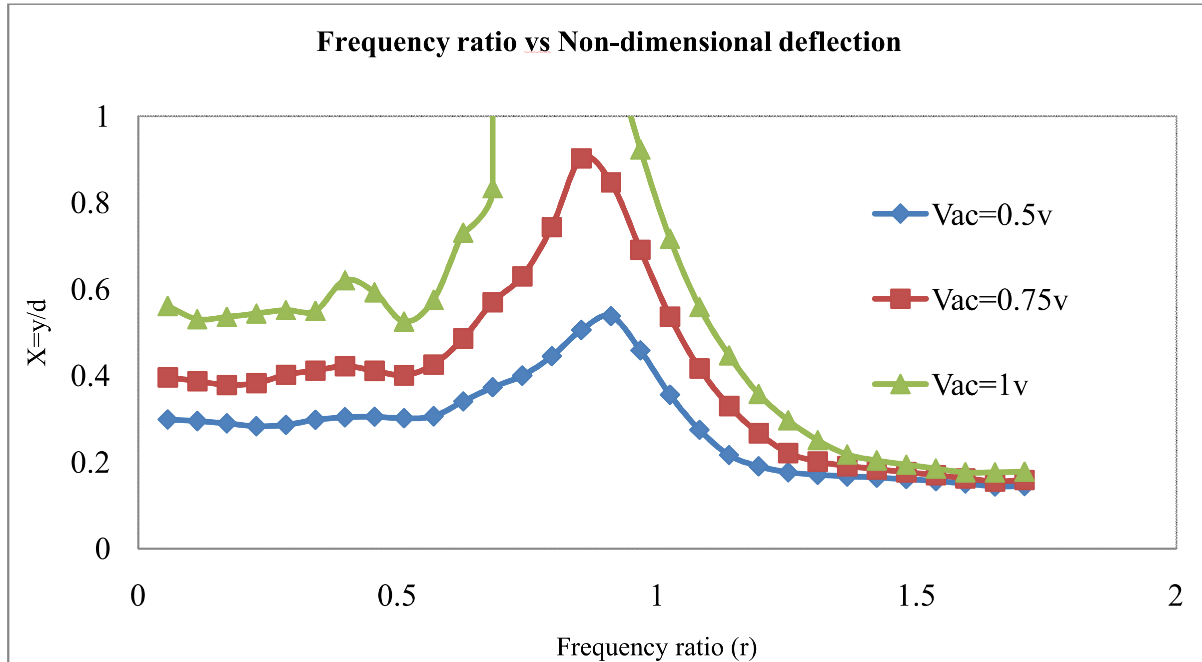

Fig.4.10 Frequency ratio vs Non-dimensional deflection
for reduced-order Galerkin model at V_{dc}=2v, pressure =800mtorr.

At three different ac voltages the frequency response curves are drawn. Here also with rise of ac voltage the amplitude of microbeam as well the peak of frequency response plot rises. For higher ac voltages, more nonlinear spring softening behaviour is observed from this figure. Table 4.1 shows the comparison of dynamic pull-in results obtained for two cases using the spring-mass model and Galerkin model. It is seen that the discrepancy occurs due several factors such as ignoring higher order terms in mode shape expansion and difference in damping expressions etc.

Tabel.4.1 Comparision of present analytic results for model 1 and model 2 micro-beams with Case1 at V_0=10v and Case 2 at V_0=1volt.

Case	Pull-in voltage		% Error
	Model 1	Model 2	
1	83.5	79.25	5.08
2	3.25	3.05	6.15

4.5 Control of chaotic dynamics

A better performance of the resonator can be achieved when the oscillations are made periodic with large amplitudes. Also the energy enhancement and subsequent increase in performance is achieved by making the system to be periodic. In present work an adaptive control approach is employed for stabilization of the system in high amplitude oscillation state. The control law can be stated as:

$$\ddot{x} = f(x, \dot{x}, t) + u$$

where u is appended control input and is given as:

$$u = -f + \ddot{x}_d + k_v(\dot{x}_d - \dot{x})$$

Here x_d is desired trajectory chosen as periodic function and k_v is a positive constant. The ac voltage amplitude is set at 2.76 volts and desired trajectory is selected as $0.3\sin 0.5\tau$. The working pressure p_0=200 mtorr and r=0.5 are maintained. Effectiveness of the controller is illustrated in Fig.4.11. It is seen that the controller is activated at time τ=25. Here k_v=2.

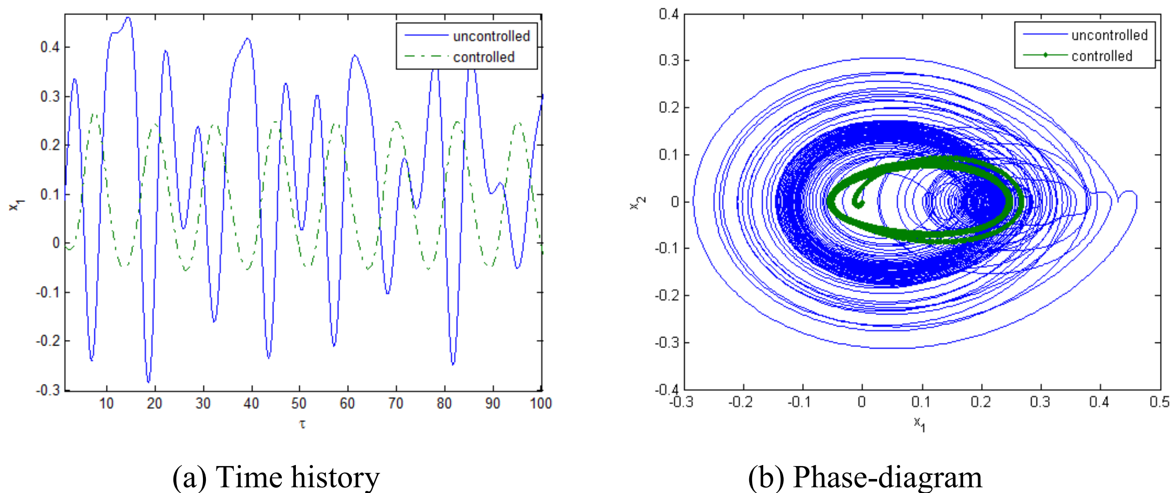

(a) Time history (b) Phase-diagram

Fig.4.11 Outputs of the controller

Motion maintains a periodic behaviour after this time.

CHAPTER-5

5. CONCLUSIONS

5.1 Summary

In this work, the results of dynamic analysis of electrostatically excited single-row cantilever micro beam resonator have been presented. Even though a lot of work has been already done in literature, present work attempted the problem in a new direction. Using both spring-mass model and the reduced-order Galerkin techniques the dynamic pull-in voltages for the two cases of microcantilever beam considered were predicted. A criterion for prediction of dynamic pull-in has been shown with reference to time-histories and phase-trajectories. Nonlinear squeeze-film model of Blench was used to model the damping along with linear viscous damping. The dependency of gap pressure on the dynamic performance of resonator has been shown. It is seen that with pressure increase, the corresponding amplitudes in frequency response reduced. Also, as other parameter, ac voltage amplitude was varied and the effects on pull-in voltage, system intermediate chaos have been predicted. The accuracy of solution from one-mode Galerkin approximation method was verified with that of single-degree of spring mass model. In summary, following things were performed:

(1) Considering a dc voltage less than that of the pull-in voltage the frequency response curves are drawn at different ac voltages. And so the effect of ac voltage on the system is investigated.
(2) The dynamic analysis results obtained from the spring –mass model are validated with that of the results obtained from reduced-order model.

Due to difference of squeeze-film damping models considered for the spring-mass model and the reduced-order Galerkin model, a variation in the dynamic pull-in voltages and the frequency responses was observed. Poincare maps were simultaneous obtained for all the cases to know the status of intermediate non-periodicity in the system is predicted.

5.2 Future work

The electrostatic forces act along the gap between micro beam and the substrate. Such an effect is known as fringing field effect. The effect of fringing field on the dynamics of microcantilever beam resonator can be included in the model as a future scope to get more accuracy. The obtained results for single-degree-of-freedom spring-mass system and reduced-order Galerkin

model may be compared with that of the multi-degree-of-freedom modeling of cantilever resonator by including damping effects. Finite element approach with mutli-physics options has to be adopted to get more insights into the resonator dynamics in micro level. Experimental characterization has to be done to predict the frequency response curves of the electrostatically excited cantilever beam model so as to know the real time damping effects on overall system dynamics. Even some of the above things were attempted; the results have not been completely obtained due to lapse of time.

REFERENCES

[1] H.M.Ouakad and M.I.Younis, 'Nonlinear Dynamics of Electrically Actuated Carbon Nanotube Resonators', *journal of computational and nonlinear dynamics*, vol.5, pp.0110099-1, 2010.

[2] Jin Woo Lee and Ryan Tung, Arvind Raman, Hartona Sumali and John P Sullivan,'Squeeze-film damping of flexible Microcantilevers at low ambient pressures: theory and experiment', *journal of micromechanics and microengineering*, vol.19,14pp, 2009.

[3] A. H.Nayfeh, M.I. Younis and E.M.Abdel-Rahman, 'Dynamic pull-in phenomenon in MEMS resonators', *Nonlinear Dyn*, vol. 48, pp.153-163, 2007.

[4] H.Yagubizade, M.Fathalilou, G.Rezazadeh and S.Talebian, 'Squeeze-Film Damping effect on dynamic Pull-in voltage of an electrostatically-actuated microbeam', Sensors *& Transducers Journal*, Vol. 103, pp.96-101, 2009.

[5] S. Huang, D.A.B. Tasiuc and J.A. Tichy, 'A simple expression for fluid inertia force acting on microplates undergoing squeeze-film damping', *Proc.R. Soc*, A, doi:10.1098/rspa.2010.0216.

[6] M.M.A. Bicak and M.D. Rao, 'Analytical modeling of squeeze-film damping for rectangular elastic plates using green's functions', *J.sound and vibration*, vol.329, pp. 4617-4633, 2010.

[7] G.D. Pasquale and A. Soma, 'Dynamic identification of electrostatically actuated MEMS in the frequency domain', Mech.system and singnal processing, vol.24, pp.1621-1633, 2010.

[8] F.M. Alsaleem, M.I. Younis and L. Ruzziconi, 'An experimental and theoretical investigation of Dynamic pull-in in MEMS resonators actuated electrostatically', *J.Micromechanical Systems*, vol.19, pp.794-805, 2010.

[9] S. Krylov, 'Lyapunov exponents as a criterion for the dynamic pull-in instability of electrostatically actuated microstructures', *Int. J. Nonlinear Mechanics*, vol.42, pp. 626-642, 2007.

[10] S. Gutschmidt, 'The influence of higher-order mode shapes for reduced-order models of electrostatically actuated microbeams', *J. Applied Mechanics*, vol.77, pp.410071-1-10, 2010.

[11] M.I.Younis and A.H.Nayfeh, 'A Study of the Nonlinear Response of a Resonant Microbeam to an Electric Actuation', *Nonlinear dynamics*, vol.31, pp.91-117, 2003.

[12] S.Chaterjee and G.Pohit [7], 'A large deflection model for the pull-in analysis of electrostatically actuated Microcantilever beams', *journal of sound and vibration*, vol.322, pp.969-986, 2009.

[13] M.I. Younis and A.H. Nayfeh, 'Simulation of squeeze-film damping of microplates actuated by large electrostatic load', *J. Computational and Nonlinear Dynamics*, Trans. AMSE, vol.2, pp.232-241, 2007.

[14] W.Zhang and G.Meng, 'Nonlinear dynamic analysis of electrostaically actuated resonant MEMS sensors under parametric excitation', *IEEE sensors journal*, vol.7, pp.370-380, 2007.

[15] S. Towfighian, G.R. Heppler and E.M. Rahman, 'Analysis of a chaotic electrostatic micro-oscillator', *J. Computational and Nonlinear Dynamics, Trans. AMSE*, vol.6, pp. 011001-1 to 10, 2011.

[16] W.Zhang and G.Meng, 'Nonlinear dynamical system of micro-cantilever under combined parametric and forcing excitations in MEMS', *Sensors and Actuators*, vol. A 119, pp. 291–299, 2005.

[17] V. Ostaseviciusa, R. Daukseviciusa, R. Gaidysb and A. Palevicius, 'Numerical analysis of fluid structure interaction effects on vibrations of cantilever microstructure', *Journal of Sound and Vibration*, vol. 308, pp. 660-673, 2007.

[18] Y.Zhang and Ya-pu Zhao, 'Numerical and analytical study on the pull-in instability of microstructure under electrostatic loading', *Sensors and Actuators* vol. A 127 pp.366–380, 2006.

[19] M. I. Younis, E.M. Abdel-Rahman, and A. Nayfeh, 'A Reduced-Order model for electrically actuated Microbeam based MEMS', *Journal Of Microelectromechanical Systems*, vol. 12, no. 5,pp.672-680, 2003.

[20] S. Chaterjee and G. Pohit, 'Squeeze-film damping characterization of cantilever microresonators for higher modes of flexural vibration', *Int. J. Engg. Science and technology*, vol.2, pp.187-199, 2010.

[21] R.C. Batra, M. Poriri and D. Spinello, 'Vibrations of narrow microbeams predeformed by an electric field', *J.Sound and Vibrations*, vol.309, pp.600-612, 2008.

[22] M. Zamanian and S.E. Khadem, 'Stability analysis of an electrically actuated microbeam using Melnikov theorm and Poincare mapping', *Proc. I Mech E., Part c, J.Mech. Engg. Science*, vol.225, pp.488-499, 2010.

[23] M.I.Ibrahim, M.I.Younis and F.Alsaleem, 'An investigation into the effects of electrostatic and squeeze-film nonlinearities on the shock spectrum of microstructures', *Int.J.Nonlinear Mechanics*, Vol.45, pp.756-765, 2010.

[24] H.S.Haghighiand and A.H.D.Markazi, 'Chaos prediction and control in MEMS resonators', *comm. Nonlinear sci numer simulat*, vol.15, pp.3091-3099,2010.

[25] F.Lakradand and M.Belhaq, 'Suppression of pull-in instability in MEMS using a high-frequency actuation', *comm. Nonlinear sci numer simulat*, vol.15, pp.3640-3646, 2010.

[26] H.T. Yau, C.C Wang, C.T. Hsieh and C.C Cho, 'Nonlinear analysis and control of uncertain MEMS by using fuzzy sliding mode controller design', *Computers & mathematics with applications*, vol.61, pp. 1912-1916, 2011.

[27] F.Alsaleem and M.I.Younis, 'Integrity analysis of electrically actuated resonators with delayed feedback controller', *J.Dynamic systems, Measurement and control, Trans.ASME*, Vol.133, pp.031011-1 to8, 2011.

APPENDIX

RUNGE-KUTTA SOLUTION FOR TIME INTEGRATION

Consider set of n-simultaneous ordinary diff. eqs in canonical form:

$$\frac{dy_1}{dt} = f_1(t, y_1, y_2, \dots y_n)$$

$$\frac{dy_2}{dt} = f_2(t, y_1, y_2, \dots y_n)$$

$$\frac{dy_n}{dt} = f_n(t, y_1, y_2, \dots y_n)$$

Expanding using 4t^h order R-K formulas we get,

$$y_{i+1,j} = y_i + \frac{1}{6}\left(k_{1j} + 2k_{2j} + 3k_{3j} + 4k_{4j}\right) + 0(h^5);\ j = 1,2,3, \dots n$$

$$k_{1j} = hf_j(t_i, y_{i1}, y_{i2}, \dots y_{in})$$

$$k_{2j} = hf_j(t_i + \frac{h}{2}, y_{i1} + \frac{k_{11}}{2}, y_{i2} + \frac{k_{12}}{2}, \dots y_{in} + \frac{k_{1n}}{2})$$

$$k_{3j} = hf_j(t_i + \frac{h}{2}, y_{i1} + \frac{k_{21}}{2}, y_{i2} + \frac{k_{22}}{2}, \dots y_{in} + \frac{k_{2n}}{2})$$

$$k_{4j} = hf_j(t_i + h, y_{i1} + \frac{k_{31}}{2}, y_{i2} + \frac{k_{32}}{2}, \dots y_{in} + \frac{k_{3n}}{2})$$

This method is programmable using nested loops.

In MATLAB, the values of *k*, *y* can be put into vectors to easily evaluate in matrix form. Following pseudo code is adopted in this work:

```
%%%%%%%%%%%%%%%%%%%%%%%%%%%%%%%%%%%%%%%%%%%%%%%%%%%
x01=0;x02=0;
r=0.5;pe=1000;
h=2*pi/r/pe;
tma=700;
i=1;
 for t0=0:h:tma
   X1(i)=x01;X2(i)=x02;
   k1=h*g1(x01,x02,t0); l1=h*g2(x01,x02,t0);
   k2=h*g1(x01+0.5*k1,x02+0.5*l1,t0+h/2);
   l2=h*g2(x01+0.5*k1,x02+0.5*l1,t0+h/2);
   k3=h*g1(x01+0.5*k2,x02+0.5*l2,t0+h/2);
   l3=h*g2(x01+0.5*k2,x02+0.5*l2,t0+h/2);
   k4=h*g1(x01+k3,x02+l3,t0+h); l4=h*g2(x01+k3,x02+l3,t0+h);
   x1n=x01+(k1+2*k2+2*k3+k4)/6; x2n=x02+(l1+2*l2+2*l3+l4)/6;
   x01=x1n;
   x02=x2n;
   i=i+1;
```

```
 end
% Generation of x1(nt) and x2(nt)
T=[0:h:tma];
for j=2*pe:pe:length(T)
  n=(j-pe)/pe;
  X3(n)=X1(n*pe);
  X4(n)=X2(n*pe);
end
%%%%%%%%%%%%%%%%%%%%%%%%%%%%%%%%%%%%%%%
```